

1 Dear Editor,

2

3 Please find below a point by point answer to the comments provided by reviewer #2. In the
4 following text, the comments of the reviewer are in written back and our answers are written in
5 blue. All the modifications suggested by the reviewer have been carefully implemented into the
6 manuscript. This updated version of the manuscript is available with the 'track changes' option at
7 the end of this file, after our answers. In addition, following the reviewer's first request, the
8 supplementary tables have also been modified and re-uploaded.

9

10 On behalf of all co-authors,

11 Goulven Laruelle

12

13 Overall statements

14 The revised manuscript "Air-water CO₂ evasion from U.S. East Coast estuaries" by Goossens, N.,
15 Gildas, L.G., Arndt, S., Wei-Jun, C., Regnier, P. has improved substantially. The authors added several
16 sections and additional tables which improved the text. Unfortunately there are still a lot of flaws in
17 the manuscript. After correcting these minor bugs I suggest to accept the manuscript for publishing
18 in Biogeosciences.

19

20 Detailed statements

21 There is still some confusion on the number of estuaries (43) handled by the model. Table S2, for
22 example, includes 40 estuaries, Table 4 has 42. I know, the problem is that some rivers enter the
23 same box. But anyway, this discrepancy in the presentation must be corrected within the entire
24 manuscript.

25 As the reviewer points out, there still were inconsistencies within the text with respect to the total
26 number of tidal estuaries simulated by the model. Table 2 is correct and the total number of systems
27 is 42. The entire manuscript has been updated accordingly and the supplementary tables (S1-S6)
28 have been updated to match the systems reported in table 2.

29

30 In the following the line numbers refer to bg-2016-278-manuscript-version4.pdf.

31

32 L558 ff and your letter to the reviewer:

33 You discuss the outgassing of small and large estuaries saying that the surface area act as a limiting
34 factor for gas exchange. Then I would expect smaller gas exchange per surface unit for smaller
35 estuaries.

36 For very small estuarine systems (such as those referred to in the discussion about the NAR region),
37 the overall surface area in the system available for the exchange between air and water is not
38 sufficient to transfer all the oversaturated CO₂ from the estuarine water to the atmosphere. In that
39 sense, surface area is a limiting factor to CO₂ outgasing because this physical limitation of the
40 available surface for gas exchange hampers the overall amount of CO₂ emitted to the atmosphere
41 during its transit through the estuarine filter. The emission rates per surface area however, are high
42 compared to other larger estuaries because the magnitude of the pCO₂ gradient at the air-water
43 interface is larger in small systems which are largely oversaturated on their entire length compared
44 to larger system where most of the outgasing only occurs in the upstream section of the estuary and
45 where the average emission rate is distributed over a much larger surface area.

46

47 L169 NAR Fig. 1; Tab. 4 includes 11 estuaries .. 558 km²

48 L174 MAR (Tab. 4) 18 entries .. 9298 km²

49 L182 SAR (Tab. 4) 13 entries .. 959 km²

50 The numbers of estuaries per region as well as their associated surface areas have been updated to
51 match the value reported in table 4. In addition, the cumulated surface areas per regions are now
52 also included in table 5.

53 L193 Friedrichs and Hofmann2001 : Reference missing
54 Both this reference and the one mentioned below were in the reference list but the line break
55 between them was missing, making the reference look like Fischer, 2001. This has been corrected in
56 the revised manuscript.
57

58 L254 Fischer 1976: Reference missing
59 Both this reference and the one mentioned above were in the reference list but the line break
60 between them was missing, making the reference look like Fischer, 2001. This has been corrected in
61 the revised manuscript.
62

63 L295 The primary production module does not include nutrients, grazing pressure, turbidity. The
64 only phytoplankton group is diatoms. Please comment on these shortenings.
65 The primary production module used in the model is described *in extenso* in Volta et al. (2014, 2016)
66 and does take into account nutrients limitations, grazing pressure and the effect of SPM
67 concentrations on water turbidity and, thus the extinction coefficient used to calculate the available
68 light in the water column. The brief description of the primary production module in the present
69 manuscript was only intended to explicit the numerical method used to integrate the light profile in
70 the water column. This short section has now been expended to clarify what processes are included
71 in the calculation of primary production in our model.
72 “The primary production dynamics, which **takes into account the combined effects of nutrients**
73 **limitation and light attenuation in the water column induced by its background turbidity and SPM**
74 **concentration**, requires vertical resolution of the photic depth. **The latter** is calculated according to
75 the method described in Vanderborght et al. (2007). This method assumes an exponential decrease
76 of the light in the water column (Platt et al., 1980), which is solved using a Gamma function.”
77

78 It is true however that our model only accounts for one phytoplankton group and that limitation as
79 well as potential future improvements are discussed in the ‘Biogeochemical Model’ paragraph of
80 section ‘3.4 Scope of applicability and model limitations’.
81 “Although the reaction network of C-GEM accounts for all processes that control estuarine FCO₂
82 (Borges and Abril, 2012; Cai, 2011), several, potentially important processes, such as benthic-pelagic
83 exchange processes, phosphorous sorption/desorption and mineral precipitation, a more complex
84 representation of the local phytoplankton community, grazing by higher trophic levels, or multiple
85 reactive organic carbon pools are not included. Although these processes are difficult to constrain
86 and their importance for FCO₂ is uncertain, the lack of their explicit representations induces
87 uncertainties in Cfilt.”
88

89 L312 World Ocean Atlas, 2009: Reference missing
90 The data from the world ocean Atlas come from Antonov et al., 2010 and Locarini et al., 2010 for the
91 temperature and salinity, respectively. This has been clarified in the manuscript:
92 “Transient physical forcings are calculated for each season and grid cell using monthly mean values
93 of water temperature (**World Ocean Atlas: Antonov et al. 2010; Locarini et al., 2010**)...”
94

95 L467 UNH/GRDC Database: give a reference
96 The following reference was added for the UNH/GRDC Database:
97 **“GRDC: Global Freshwater Fluxes into the World Oceans / Online provided by Global Runoff Data**
98 **Centre. 2014 ed. Koblenz: Federal Institute of Hydrology (BfG), 2014.”**
99

100 L468 Fekete et al 2000: Reference missing

101 The Fekete et al 2000 reference was removed and replaced by GRDC (2014) to refer to the
102 UNH/GRDC Database (see comment above).
103
104 L473 is it July 2003 or July 2013? Compare L487
105 The validation performed for the Delaware Bay relies on a pH longitudinal profile and boundary
106 conditions all sampled in 2003 (Sharp et al., 2009; Sharp, 2010) as stated in the manuscript.
107 However, for comparison's sake, a reference is also made to the recent work of Joesoef et al. (2015)
108 when discussing the pCO₂ profile because this study reports pCO₂ measurements performed in the
109 same estuary during the same month (July) but another year (2013). The fact that Joesoef et al.
110 (2015)'s data were not sampled the same year as the one simulated by the model was already
111 mentioned in the text, but the following sentences have been modified to make this fact clearer and
112 avoid potential confusion:
113 **"Overall, the longitudinal pCO₂ profile of the Delaware estuary is characterized by** values close to
114 equilibrium with the atmosphere in the widest section of the Delaware Bay (close to the estuarine
115 mouth **and throughout the 40 first kilometers of the system**) and values above 1200 μatm at
116 **kilometer 150 and beyond, where characteristic** salinities **are** below 5. **Although the profile**
117 **presented here is simulated using boundary conditions representative of July 2003 and no pCO₂**
118 **data were available for validation for this period, a recent study by Joesoef et al. (2015) reports a**
119 **similar longitudinal pCO₂ profile in July 2013.**"
120
121 L481 I think you exchanged the display of pH upstream and downstream in the tables, as they do not
122 fit to Fig. 7
123 There was indeed in mistake in table S6 displaying the pH values used at the downstream boundary
124 condition, which are calculated from DIC and Alkalinity assuming CO₂ equilibrium between coastal
125 waters and the atmosphere (see section 2.4.4 of the manuscript). Table S6 was updated with the
126 proper values. Table S5, which provides the upstream boundary conditions, was correct however.
127
128 L490 Compare pCO₂ along the salinity gradient, or change text here.
129 Panel c of figure 7 reports simulated pCO₂ values for the Delaware estuary against the distance from
130 the mouth of the system. When discussing this profile, we now refer the distance from the estuarine
131 mouth rather than to salinity to identify the different sections of the estuary:
132 **"Overall, the longitudinal pCO₂ profile of the Delaware estuary is characterized by** values close to
133 equilibrium with the atmosphere in the widest section of the Delaware Bay (**near** the estuarine
134 mouth **and throughout the 40 first kilometers of the system**) and values above 1200 μatm at
135 **kilometer 150 and beyond, where characteristic** salinities **are** below 5."
136
137 L500 "Although .." Improve grammar.
138 The sentence was rewritten as:
139 **"Although *significant* discrepancies *are observed* at the level of individual systems, the model**
140 **captures remarkably well the overall *behaviors of estuaries along the East coast of the US in term***
141 **of intensity of** CO₂ evasion rate."
142
143 L501 is it really a trend?
144 The use of the word tend was not really adequate in this sentence and it was removed in the
145 updated manuscript (see comment above).
146
147 L502 I see only 6 systems
148 If Florida Bay is removed from table 2, as suggested by the reviewer in his third to last comment,
149 there indeed will be only 6 systems with observed emission rates < 5 mol C m⁻² yr⁻¹.
150
151 L503 I see only 5 systems

152 Indeed, the reviewer is correct; there are only 5 systems with observed emission rates $> 10 \text{ mol C m}^{-2} \text{ yr}^{-1}$.
153 The sentence was corrected in the manuscript.
154 “The model simulates low CO_2 efflux ($< 5 \text{ mol C m}^{-2} \text{ yr}^{-1}$) for the 6 systems where such conditions have
155 been observed, while the 5 systems for which the CO_2 evasion exceeds $10 \text{ mol C m}^{-2} \text{ yr}^{-1}$ are the
156 same in the observations and in the model runs.”
157
158 L507 “local observations”
159 Corrected
160
161 L544 “B0”
162 Corrected
163
164 L468 Savenije 2000: Reference missing
165 The reference was intended to be Savenije (2005), which is in the reference list. This mistake was
166 corrected in the updated manuscript.
167 “A larger ratio of estuarine width B0 and convergence length b corresponds to a more funnel shaped
168 estuary while a low ratio corresponds to a more prismatic geometry (Savenije, 2005; Volta et al.,
169 2014).”
170
171 L564 “2013b”
172 Corrected
173
174 L567 Zeebe and Wolf-Gladrow 2001: Reference missing
175 The reference has been added to the reference list:
176 “Zeebe, R. E. and Wolf-Gladrow, D. (Eds.): CO2 in seawater: equilibrium, kinetics, isotopes, Elsevier, Amsterdam, 2001.”
177
178
179 L717 “discuss”
180 Corrected
181
182 L721 “watersheds”
183 Corrected
184
185 L723 “contained by” -> “covered by”
186 Corrected
187
188 L730 (b, B0, H)
189 Corrected
190
191 L772 omit “is”
192 Corrected
193
194 L789 Antonov et al., 2014: Reference missing
195 Although the database has been updated in 2014, the recommended reference is Antonov et al.,
196 2010, which is in our reference list. The text was updated accordingly:
197 “At the lower boundary condition, direct observations for nutrients and oxygen are extracted from
198 databases such as the World Ocean Atlas (Antonov et al., 2010).”
199
200 L802 “Chlorophyll-a”
201 Corrected
202

203 L802 omit "and" -> "For DIC and alkalinity boundary conditions .."
204 Corrected
205
206 L804 "are extracted"
207 Corrected
208
209 L812-815 Improve grammar.
210 The sentence was rewritten as:
211 "The generic nature of the applied model approach *renders a direct validation of model results on*
212 *the basis of local and instantaneous observational data (e.g. longitudinal profiles) difficult.* In
213 particular the applications of seasonally/annually averaged or model-deduced boundary conditions,
214 which are likely not representative of these long-term average conditions, *do not lend themselves*
215 *well to comparison with punctual measurements.*"
216
217 L841 Mayer and Eyre, 2012: Reference missing
218 The proper citation was Maher and Eyre, 2012. This typo was corrected in the manuscript and
219 Maher and Eyre (2012) is in the reference list.
220
221 L897 "suggests"
222 Corrected
223
224 L967 Abril 2002 does not fit to L39
225 Abril (2002) is not cited in L39, Borges and Abril (2012) is.
226
227 L998 Billen et al: Not called
228 The reference above was removed from the reference list.
229
230 L1062 Hartmann 2012 does not fit to L165
231 Hartmann (2012) is not cited in L165, Hartmann et al. (2009) is.
232
233 L1176 Paerl et al: Not called
234 L1262 Thieu et al: Not called
235 L1282 Van der Burgh: Not called
236 The three references above were removed from the reference list.
237
238 L1306 Tab. 2 omit Florida Bay as this was not modeled.
239 Florida Bay has been removed from table 2 and the corresponding reference (Dufore et al., 2012)
240 has been removed from the reference list.
241
242 L1353 In the text you discuss Fig. 7b as Delaware (L486).
243 This is indeed a mistake, the pCO₂ profile for the Delaware estuary is represented in panel c. The text
244 has been updated accordingly.
245 "Both processes lead to a well-developed pCO₂ increase in this area (Fig. 7c)."
246
247 L1378 -FCO₂ should be also at the y-axis
248 The caption is wrong and not the axis. Instead of referring to NEM and -FCO₂, the caption should
249 refer to -NEM and FCO₂. It has been updated accordingly in the manuscript.
250 "Panels b, d and e represent -NEM, FCO₂ and C_{Filt}, respectively. Panels a and c represent -NEM,
251 FCO₂ normalized by a temperature Q₁₀ function."
252
253

254

Air-water CO₂ evasion from U.S. East Coast estuaries

255 Goossens, Nicolas¹, Laruelle, Goulven Gildas^{1*}, Arndt, Sandra², Cai, Wei-Jun³ & Regnier, Pierre¹

256

257 1 Department Geosciences, Environment and Society, Université Libre de Bruxelles, Brussels,
258 Belgium

259 2 School of Geographical Sciences, University of Bristol, Bristol, UK

260 3 School of Marine Science and Policy, University of Delaware, Newark, Delaware, USA

261

262 *corresponding author: goulven.gildas.laruelle@ulb.ac.be

263

264

265 **Abstract:**

266 This study presents the first regional-scale assessment of estuarine CO₂ evasion along the East coast
267 of the US (25 – 45 °N). The focus is on 42 tidal estuaries, which together drain a catchment of
268 697000 km² or 76 % of the total area within this latitudinal band. The approach is based on the
269 Carbon – Generic Estuarine Model (C-GEM) that allows simulating hydrodynamics, transport and
270 biogeochemistry for a wide range of estuarine systems using readily available geometric parameters
271 and global databases of seasonal climatic, hydraulic, and riverine biogeochemical information. Our
272 simulations, performed using conditions representative of the year 2000, suggest that, together, US
273 East coast estuaries emit 1.9 TgC yr⁻¹ in the form of CO₂, which correspond to about 40 % of the
274 carbon inputs from rivers, marshes and mangroves. Carbon removal within estuaries results from a
275 combination of physical (outgassing of supersaturated riverine waters) and biogeochemical
276 processes (net heterotrophy and nitrification). The CO₂ evasion and its underlying drivers show
277 important variations across individual systems, but reveal a clear latitudinal pattern characterized by
278 a decrease in the relative importance of physical over biogeochemical processes along a North-South
279 gradient. Finally, the results reveal that the ratio of estuarine surface area to the river discharge, S/Q
280 (which has a scale of per meter discharged water per year), could be used as a predictor of the
281 estuarine carbon processing in future regional and global scale assessments.

Deleted: 43

283 **1 Introduction**

284 Carbon fluxes along the land-ocean aquatic continuum are currently receiving increasing attention
285 because of their recently recognized role in the global carbon cycle and anthropogenic CO₂ budget
286 (Bauer et al., 2013; Regnier et al., 2013a; LeQuéré et al., 2014, 2015). Estuaries are important
287 reactive conduits along this continuum, which links the terrestrial and marine global carbon cycles
288 (Cai, 2011). Large amounts of terrestrial carbon transit through these systems, where they mix with
289 carbon from autochthonous, as well as marine sources. During estuarine transit, heterotrophic
290 processes degrade a fraction of the allochthonous and autochthonous organic carbon inputs,
291 supporting a potentially significant, yet poorly quantified CO₂ evasion flux to the atmosphere. Recent
292 estimates suggest that 0.15-0.25 PgC yr⁻¹ is emitted from estuarine systems worldwide (Borges and
293 Abril, 2012; Cai, 2011; Laruelle et al., 2010; Regnier et al., 2013a; Laruelle et al., 2013, Bauer et al.,
294 2013). Thus, in absolute terms the global estuarine CO₂ evasion corresponds to about 15% of the
295 open ocean CO₂ uptake despite the much smaller total surface area.

296 Currently, estimates of regional and global estuarine CO₂ emissions are mainly derived on the basis
297 of data-driven approaches that rely on the extrapolation of a small number of local measurements
298 (Cai, 2011; Chen et al., 2013; Laruelle et al., 2013). These approaches fail to capture the spatial and
299 temporal heterogeneity of the estuarine environment (Bauer et al., 2013) and are biased towards
300 anthropogenically influenced estuarine systems located in industrialized countries (Regnier et al.,
301 2013a). Even in the best surveyed regions of the world (e.g. Australia, Western Europe, North
302 America or China) observations are merely available for a small number of estuarine systems. In
303 addition, if available, data sets are generally of low spatial and temporal resolution. As a
304 consequence, data-driven approaches can only provide first-order estimates of regional and global
305 estuarine CO₂ emissions.

306 Integrated model-data approaches can help here, as models provide the means to extrapolate over
307 temporal and spatial scales and allow disentangling the complex and very dynamic network of

308 physical and biogeochemical processes that controls estuarine CO₂ emissions. Over the past
309 decades, increasingly complex process-based models have been applied, in combination with local
310 data, to elucidate the coupled carbon-nutrient cycles on the scale of individual estuaries (e.g.,
311 O’Kane, 1980; Soetaert and Herman, 1995; Vanderborght et al., 2002; Lin et al., 2007; Arndt et al.,
312 2009; Cerco et al., 2010; Baklouti et al., 2011). However, the application of such model approaches
313 remains limited to the local scale due to their high data requirements for calibration and validation
314 (e.g. bathymetric and geometric information and boundary conditions), as well as the high
315 computational demand associated with resolving the complex interplay of physical and
316 biogeochemical processes on the relevant temporal and spatial scales (Regnier et al., 2013b).
317 Complex process-based models are thus not suitable for the application on a regional or global scale
318 and, as a consequence, the estuarine carbon filter is, despite its increasingly recognized role in
319 regional and global carbon cycling (e.g. Bauer et al., 2013), typically not taken into account in model-
320 derived regional or global carbon budgets (Bauer et al., 2013). The lack of regional and global model
321 approaches that could be used as stand-alone applications or that could be coupled to regional
322 terrestrial river network models (e.g. GLOBALNEWS: Seitzinger et al., 2005; Mayorga et al., 2010;
323 SPARROW: Schwarz et al., 2006) and continental shelf models (e.g. Hofmann et al., 2011) is thus
324 critical.

325 The Carbon-Generic Estuary Model (C-GEM (v1.0); Volta et al., 2014) has been developed with the
326 aim of providing such a regional/global modeling tool that can help improve existing, observationally
327 derived first order estimates of estuarine CO₂ emissions. C-GEM (v1.0) has been specifically designed
328 to reduce data requirements and computational demand and, thus, tackles the main impediments
329 for the application of estuarine models on a regional or global scale. The approach takes advantage
330 of the mutual dependency between estuarine geometry and hydrodynamics in alluvial estuaries
331 and uses an idealized representation of the estuarine geometry to support the hydrodynamic
332 calculations. It thus allows running steady state or fully transient annual to multi-decadal simulations
333 for a large number of estuarine systems, using geometric information readily available through maps

334 or remote sensing images. Although the development of such a regional/global tool inevitably
335 requires simplification, careful model evaluations have shown that, despite the geometric
336 simplification, C-GEM provides an accurate description of the hydrodynamics, transport and
337 biogeochemistry in tidal estuaries (Volta et al., 2014). In addition, the model approach was
338 successfully used to quantify the contribution of different biogeochemical processes for CO₂ air-
339 water fluxes in an idealized, funnel-shaped estuary forced by typical summer conditions
340 characterizing a temperate Western European climate (Regnier et al., 2013b). Volta et al. (2016b)
341 further investigated the effect of estuarine geometry on the CO₂ outgassing using three idealized
342 systems and subsequently established the first regional carbon budget for estuaries surrounding the
343 North Sea by explicitly simulating the six largest systems of the area (Volta et al., 2016a), including
344 the Scheldt and the Elbe for which detailed validation was performed.

345 Here, we extend the domain of application of C-GEM (v1.0) to quantify CO₂ exchange fluxes, as well
346 as the overall organic and inorganic carbon budgets for the full suite of estuarine systems located
347 along the entire East coast of the United States, one of the most intensively monitored regions in the
348 world. A unique set of regional data, including partial pressure of CO₂ in riverine and continental
349 shelf waters (pCO₂; Signorini et al., 2013; Laruelle et al., 2015), riverine biogeochemical
350 characteristics (Lauerwald et al., 2013), estuarine eutrophication status (Bricker et al., 2007) and
351 estuarine morphology (NOAA, 1985) are available. These comprehensive data sets are
352 complemented by local observations of carbon cycling and CO₂ fluxes in selected, individual
353 estuarine systems (see Laruelle et al., 2013 for a review), making the East coast of the United States
354 an ideal region for a first, fully explicit regional evaluation of CO₂ evasion resolving every major tidal
355 estuary along the selected coastal segment. The scale addressed in the present study is
356 unprecedented so far (> 3000 km of coastline) and covers a wide range of estuarine morphological
357 features, climatic conditions, land-use and land cover types, as well as urbanization levels. The
358 presented study will not only allow a further evaluation of C-GEM (v1.0), but will also provide the
359 first regional-scale assessment of estuarine CO₂ evasion along the East coast of the US (25 – 45 °N)

360 and will help explore general relationships between carbon cycling and CO₂ evasion, and readily
361 available estuarine geometrical parameters.

362 After a description of the model itself and of the dataset used to set up the simulations, a local
363 validation is presented which includes salinity, pCO₂ and pH longitudinal profiles for two well
364 monitored systems (the Delaware Bay and the Altamaha River Estuary). The yearly averaged rates of
365 CO₂ exchange at the air-water interface simulated by the model for 13 individual estuaries are also
366 compared with observed values reported in the literature. Next, regional scale simulations for 42
367 tidal estuaries of the eastern US coast provide seasonal and yearly integrated estimates of the Net
368 Ecosystem Metabolism (NEM), CO₂ evasion and carbon filtering capacity, CFilt. Model results are
369 then used to elucidate the estuarine biogeochemical behavior along the latitudinal transect
370 encompassed by the present study (30-45° N). Finally, our results are used to derive general
371 relationships between carbon cycling and CO₂ evasion, and readily available estuarine geometrical
372 parameters.

Deleted: 3

373

374 **2. Regional description and model approach**

375 **2.1 Observation-based carbon budget for the East coast of the United States**

376 The study area covers the Atlantic coast of the United States (Fig.1), from the southern tip of Florida
377 (25°N) to Cobscook Bay (45°N) at the US-Canada boundary. This area encompasses distinct climatic
378 zones and land cover types and exhibits a variety of morphologic features (Fig. 1). The region can be
379 subdivided into several sub-regions following a latitudinal gradient (Signorini et al., 2013). In this
380 study, we define three sub-regions following the boundaries suggested by the COSCAT segmentation
381 (Meybeck et al., 2006; Laruelle et al., 2013) and the further subdivision described in Laruelle et al.
382 (2015). From North to South, the regions are called North Atlantic, Mid Atlantic and South Atlantic
383 Regions (Fig. 1). Total carbon inputs from watersheds to US East coast estuaries (Tab. 1) have been

385 estimated to range from 4.0 to 10.7 Tg C yr⁻¹ (Mayorga et al., 2010; Shih et al., 2010; Stets and Strieg,
386 2012; Tian et al., 2010; Tian et al., 2012), consisting of dissolved organic carbon (DOC; ~50%),
387 dissolved inorganic carbon (DIC; ~40%) and particulate organic carbon (POC; ~10%). In addition, a
388 statistical approach has been applied to estuaries of the region to quantify organic carbon budgets
389 and Net Ecosystem Productivity (NEP) using empirical models (Herrmann et al., 2015).

390 Recent studies estimated that, along the East coast of the United States, rivers emit 11.4 TgC yr⁻¹ of
391 CO₂ to the atmosphere (Raymond et al., 2013), while continental shelf waters absorb between 3.4
392 and 5.4 TgC yr⁻¹ of CO₂ from the atmosphere (Signorini et al., 2013). A total of thirteen local, annual
393 mean estuarine CO₂ flux estimates across the air-water interface based on measurements are also
394 reported in the literature and are grouped along a latitudinal gradient (Tab. 2). Four of these
395 estimates are located in the South Atlantic region (SAR): Sapelo Sound, Doboy Sound, Altamaha
396 Sound (Jiang et al., 2008), and the Satilla River estuary (Cai and Wang, 1998). Three studies
397 investigate CO₂ fluxes in the mid-Atlantic Region (MAR): the York River Estuary (Raymond et al.,
398 2000) and the Hudson River (Raymond et al., 1997). There is also a comprehensive CO₂ flux study for
399 the Delaware Estuary published after the completion of this work (Joeseof et al., 2015). Six systems
400 are located in the North Atlantic region (NAR): The Great Bay, the Little Bay, the Oyster estuary, the
401 Bellamy estuary, the Cocheco estuary (Hunt et al., 2010; 2011), and the Parker River estuary
402 (Raymond and Hopkinson, 2003). The mean annual flux per unit area from these local studies is
403 11.7±13.1 mol C m⁻² yr⁻¹ and its extrapolation to the total estuarine surface leads to a regional CO₂
404 evasion estimate of 3.8 Tg C y⁻¹. This estimate is in line with that of Laruelle et al. (2013) for the same
405 region which proposes an average CO₂ emission rate of 10.8 mol C m⁻² yr⁻¹. Thus, CO₂ outgassing
406 could remove 35% to 95% of the riverine carbon loads during estuarine transit. About 75 % of the
407 air-water exchange occurs in tidal estuaries (2.8 Tg C y⁻¹) while lagoons and small deltas contribute to
408 the remaining 25 %. Although these simple extrapolations from limited observational data are
409 associated with large uncertainties, they highlight the potentially significant contribution of estuaries
410 to the CO₂ outgassing in the region. However, process-based quantifications of regional organic and

411 inorganic C budgets including air-water CO₂ fluxes for the estuarine systems along the East coast are
412 not available.

413 2.2 Selection of estuaries

414 The National Estuarine Eutrophication Assessment (NEEA) survey (Bricker et al., 2007), which uses
415 geospatial data from the National Oceanic and Atmospheric Administration (NOAA) Coastal
416 Assessment Framework (CAF) (NOAA, 1985), was used to identify and characterize 58 estuarine

417 systems discharging along the Atlantic coast of the United States. From this set, ~~42~~ 16 'tidal' estuaries,
418 defined as a river stretch of water that is tidally influenced (Dürr et al., 2011), were retained (Fig. 1)
419 to be simulated by the C-GEM model, which is designed to represent such systems. Using outputs
420 from terrestrial models (Hartmann et al., 2009; Mayorga et al., 2010), the cumulated riverine carbon
421 loads for all the non-tidal estuaries that are excluded from the present study amount to 0.9 Tg C yr⁻¹,

422 which represents less than 15% of the total riverine carbon loads of the region. These ~~16~~ 16 systems are
423 located in the SAR (10) and in the MAR (~~6~~).

424 The northeastern part of the domain (NAR, Fig. 1; Tab. 1) includes ~~11~~ 11 estuaries along the Gulf of
425 Maine and the Scotian shelf, covering a cumulative surface area of ~~558~~ 558 km². It includes drowned
426 valleys, rocky shores and a few tidal marshes. The climate is relatively cold (annual mean= 8°C) and
427 the human influence is relatively limited because of low population density and low freshwater
428 inputs. The mean estuarine water depth is 12.9 m and the mean tidal range is 2.8 m.

429 The central zone (MAR) includes ~~18~~ 18 tidal estuaries accounting for a total surface area of ~~9298~~ 9298 km².
430 The Chesapeake Bay and the Delaware estuaries alone contribute more than 60% to the surface area
431 of the region. In this region, estuaries are drowned valleys with comparatively high river discharge
432 and intense exchange with the ocean. Several coastal lagoons, characterized by a limited exchange
433 with the ocean are located here, but are not included in our analysis. The Mid-Atlantic Region (MAR)
434 is characterized by a mean annual temperature of 13°C and is strongly impacted by human activities,

Deleted: 43

Deleted: 15

Deleted: 5

Deleted: 20

Deleted: ~5300

Deleted: 17

Deleted: 14500

442 due to the presence of several large cities (e.g. New York, Washington, Philadelphia, Baltimore) and
443 intense agriculture. The mean water depth is about 4.7 m and the tidal range is 0.8 m.

444 The southern Atlantic region (SAR) includes 13 tidal estuaries covering a total surface area of 959
445 km². These systems are generally dendritic and surrounded by extensive salt marshes. The climate is
446 subtropical with an average annual temperature of 19°C. Land use includes agriculture and industry,
447 but the population density is generally low. Estuarine systems in the SAR are characterized by a
448 shallow mean water depth of 2.9 m and a tidal range of 1.2 m.

Deleted: 10

Deleted: 12182

449 **2.3 Model set-up**

450 The generic 1D Reactive-Transport Model (RTM) C-GEM (Volta et al., 2014) is used to quantify the
451 estuarine carbon cycling in the 42 systems considered in this study. The approach is based on
452 idealized geometries (Savenije, 2005; Volta et al., 2014) and is designed for regional and global scale
453 applications (Regnier et al., 2013b; Volta et al., 2014, 2016a). The model approach builds on the
454 premise that hydrodynamics exerts a first-order control on estuarine biogeochemistry (Arndt et al.,
455 2007; Friedrichs and Hofmann, 2001) and CO₂ fluxes (Regnier et al., 2013a). The method takes
456 advantage of the mutual dependence between geometry and hydrodynamics in tidal estuaries
457 (Savenije, 1992) and the fact that, as a consequence, transport and mixing can be easily quantified
458 from readily available geometric data (Regnier et al., 2013a; Savenije, 2005; Volta et al., 2016b).

Deleted: 43

459 **2.3.1 Description of idealized geometries for tidally-averaged conditions**

460 Although tidal estuaries display a wide variety of shapes, they nevertheless share common
461 geometric characteristics that are compatible with an idealized representation (Fig. 2, Savenije,
462 1986; Savenije, 2005). For tidally-averaged conditions, their width B (or cross-sectional area A) can
463 be described by an exponential decrease as a function of distance, x, from the mouth (Savenije,
464 1986; Savenije, 2005):

$$B = B0 * \exp\left(-\frac{x}{b}\right) \quad (1)$$

468 where B (m) is the tidally averaged width, B0 (m) the width at the mouth, x (m) the distance from
 469 the mouth (x=0) and b (m) the width convergence length (Fig. 2). The width convergence length, b, is
 470 defined as the distance between the mouth and the point at which the width is reduced to B0 e⁻¹. It
 471 is directly related to the dominant hydrodynamic forcing. A high river discharge typically results in a
 472 prismatic channel with long convergence length (river dominated estuary), while a large tidal range
 473 results in a funnel-shaped estuary with short convergence length (marine dominated estuary). At the
 474 upstream boundary, the estuarine width is given by:

$$B_L = B0 * \exp\left(-\frac{L}{b}\right) \quad (2)$$

475 Where L denotes the total estuarine length (m) along the estuarine longitudinal axis.

476 The total estuarine surface S (m²) can be estimated by integrating equation (1) over the estuarine
 477 length:

$$S = \int_0^L B dx = b * B0 * \left(1 - \exp\left(-\frac{L}{b}\right)\right) \quad (3)$$

478

479 The width convergence length is then calculated from B0, B_L, L and the real estuarine surface area
 480 (SR) by inserting equation (2) in equation (3):

$$b = \frac{SR}{B0 - B_L} \quad (4)$$

481 SR is calculated for each system using the SRTM water body data (Fig. 3a), a geographical dataset
 482 encoding high-resolution worldwide coastal outlines in a vector format (NASA/NGA, 2003). While
 483 such a database exists for a well monitored region such as the East coast of the US, resorting to
 484 using the idealized estuarine surface area (S) is necessary in many other regions. The longitudinal

485 mean, tidally averaged, depth h (m), is obtained from the National Estuarine Eutrophication
 486 Assessment database (Bricker et al., 2007).

487 Using this idealized representation, the estuarine geometry can be defined by a limited number of
 488 parameters: the width at the mouth (B_0), the estuarine length (L), the estuarine width at the
 489 upstream limit (B_L) and the mean depth h . These parameters can be easily determined from local
 490 maps or Google Earth using Geographic Information Systems (GIS) or obtained from databases
 491 (NASA/NGA, 2003).

492 2.3.2 Hydrodynamics, transport and biogeochemistry

493 Estuarine hydrodynamics are described by the one-dimensional barotropic, cross-sectionally
 494 integrated mass and momentum conservation equations for a channel with arbitrary geometry
 495 (Nihoul and Ronday, 1976; Regnier et al., 1998; Regnier and Steefel, 1999):

$$496 \quad r_s \frac{\partial A}{\partial t} + \frac{\partial Q}{\partial x} = 0 \quad (5)$$

$$497 \quad \frac{\partial U}{\partial t} + U \frac{\partial U}{\partial x} = -g \frac{\partial \zeta}{\partial x} - g \frac{U|U|}{C_z^2 H} \quad (6)$$

498 where:

499	t	time	[s]
500	x	distance along the longitudinal axis	[m]
501	A	cross-section area $A = H \cdot B$	[m ²]
502	Q	cross-sectional discharge $Q = A \cdot U$	[m ³ s ⁻¹]
503	U	flow velocity Q / A	[m s ⁻¹]
504	r_s	storage ratio $r_s = B_s / B$	[-]

505	B_s	storage width	[m]
506	g	gravitational acceleration	[m s ⁻²]
507	ξ	elevation	[m]
508	H	total water depth $H = h + \xi(x, t)$	[m]
509	C_z	Chézy coefficient	[m ^{1/2} s ⁻¹]

510 The coupled partial differential equations (Eqs. (5) and (6)) are solved by specifying the elevation
511 $\xi_0(t)$ at the estuarine mouth and the river discharge $Q_0(t)$ at the upstream limit of the model domain.

512 The one-dimensional, tidally-resolved, advection-dispersion equation for a constituent of
513 concentration $C(x, t)$ in an estuary can be written as (e.g. Pritchard, 1958):

$$514 \quad \frac{\partial C}{\partial t} + \frac{Q}{A} \frac{\partial C}{\partial x} = \frac{1}{A} \frac{\partial}{\partial x} \left(AD \frac{\partial C}{\partial x} \right) + P \quad (7)$$

515 where $Q(x, t)$ and $A(x, t)$ denote the cross-sectional discharge and area, respectively and are provided
516 by the hydrodynamic model (eq. 5 and 6). $P(x, t)$ is the sum of all production and consumption
517 process rates affection the concentration of the constituent. The effective dispersion coefficient D
518 (m² s⁻¹) implicitly accounts for dispersion mechanisms associated to sub-grid scale processes (Fischer,
519 1976; Regnier et al., 1998). In general, D is maximal near the sea, decreases upstream and becomes
520 virtually zero near the tail of the salt intrusion curve (Preddy, 1954; Kent, 1958; Ippen and Harleman,
521 1961; Stigter and Siemons, 1967). The effective dispersion at the estuarine mouth can be quantified
522 by the following relation (Savenije, 1986):

$$523 \quad D_0 = 26 \cdot (h_0)^{1.5} \cdot (N \cdot g)^{0.5} \quad (8)$$

524 where h_0 (m) is the tidally-averaged water depth at the estuarine mouth and N is the dimensionless
525 Canter Cremers' estuary number defined as the ratio of the freshwater entering the estuary during a

526 tidal cycle to the volume of salt water entering the estuary over a tidal cycle (Simmons, 1955).

$$527 \quad N = \frac{Q_b \cdot T}{P} \quad (9)$$

528 In this equation, Q_b is the bankfull discharge ($\text{m}^3 \text{s}^{-1}$), T is the tidal period (s) and P is the tidal prism
529 (m^3). For each estuary, N can thus be calculated directly from the hydrodynamic model. The
530 variation in D along the estuarine gradient can be described by Van der Burgh's equation (Savenije,
531 1986):

$$532 \quad \frac{\partial D}{\partial x} = -K \frac{Q_r}{A} \quad (10)$$

533 where K is the dimensionless Van der Burgh's coefficient and the minus sign indicates that D
534 increases in downstream direction (Savenije, 2012). The Van der Burgh's coefficient is a shape factor
535 that has values between 0 and 1 (Savenije, 2012), and is a function of estuarine geometry for tidally
536 average conditions. Therefore, each estuarine system has its own characteristic K value, which
537 correlates with geometric and hydraulic scales (Savenije, 2005). Based on a regression analysis
538 covering a set of 15 estuaries, it has been proposed to constrain K from the estuarine geometry
539 (Savenije, 1992):

$$540 \quad K = 4.32 \cdot \frac{h_0^{0.36}}{B_0^{0.21} \cdot b^{0.14}} \quad \text{with } 0 < K < 1 \quad (11)$$

541 Reaction processes P considered in C-GEM comprise aerobic degradation, denitrification,
542 nitrification, primary production, phytoplankton mortality and air-water gas exchange for O_2 and CO_2
543 (Fig. 4 and Tab. 3). These processes and their mathematical formulation are described in detail in
544 Volta et al. (2014) and Volta et al. (2016a).

545 The non-linear partial differential equations for the hydrodynamics are solved by a finite difference
546 scheme following the approach of (Regnier et al., 1997; Regnier and Steefel, 1999) and
547 (Vanderborcht et al., 2002). The timestep Δt is 150s and the grid size Δx is constant along the

548 longitudinal axis of the estuary. The grid size default value is 2000 m, but can be smaller for short
549 length estuaries to guarantee a minimum of 20 grid points within the computational domain.
550 Transport and reaction terms are solved in sequence within a single timestep using an operator
551 splitting approach (Regnier et al., 1997). The advection term in the transport equation is integrated
552 using a third-order accurate total variation diminishing (TVD) algorithm with flux limiters (Regnier et
553 al., 1998), ensuring monotonicity (Leonard, 1984), while a semi-implicit Crank-Nicholson algorithm is
554 used for the dispersion term (Press et al., 1992). These schemes have been extensively tested using
555 the CONTRASTE estuarine model (e.g. Regnier et al., 1998; Regnier and Steefel, 1999; Vanderborght
556 et al., 2002) and guarantee mass conservation to within <1%. The reaction network (including
557 erosion-deposition terms when the constituent is a solid species), is numerically integrated using the
558 Euler method (Press et al., 1992). The primary production dynamics, which takes into account the
559 combined effects of nutrients limitation and light attenuation in the water column induced by its
560 background turbidity and SPM concentration, requires vertical resolution of the photic depth. The
561 latter is calculated according to the method described in Vanderborght et al. (2007). This method
562 assumes an exponential decrease of the light in the water column (Platt et al., 1980), which is solved
563 using a Gamma function.

Deleted: ,

Deleted: is

564 2.4 Boundary and forcing conditions

565 Boundary and forcing conditions are extracted from global databases and global model outputs that
566 are available at 0.5° resolution. Therefore, C-GEM simulations are performed at the same resolution
567 according to the following procedure. First, 42 coastal cells corresponding to tidal estuaries are
568 identified in the studied area (Fig. 1). If the mouth of an estuary is spread over several 0.5° grid cells,
569 those cells are regrouped in order to represent a single estuary (e.g. Delaware estuary), and
570 subsequently, a single idealized geometry is defined as described above. The model outputs
571 (Hartmann et al. , 2009; Mayorga et al., 2010) and databases (Antonov et al., 2010; Garcia et al.,

Deleted: 43

575 2010a; Garcia et al., 2010b) used to constrain our boundary conditions are representative of the
576 year 2000.

577 For each resulting cell, boundary and forcing conditions are calculated for the following periods:
578 January-March; April-June; July-September and October-December. This allows for an explicit
579 representation of the seasonal variability in the simulations.

580 **2.4.1 External forcings**

581 Transient physical forcings are calculated for each season and grid cell using monthly mean values of
582 water temperature (World Ocean Atlas: [Antonov et al. 2010](#); [Locarini et al., 2010](#)) and seasonal
583 averaged values for wind speed (Cross-Calibrated-Multi-Platform (CCMP) Ocean Surface Wind
584 Vector Analyses project (Atlas et al., 2011)). Mean daily solar radiation and photoperiods (corrected
585 for cloud coverage using the ISCCP Cloud Data Products, Rossow and Schiffer, 1999) are calculated
586 depending on latitude and day of the year using a simple model (Brock, 1981).

Formatted: Not Highlight

Deleted: , 2009

Formatted: Highlight

587 **2.4.2 Riverine discharge, concentrations and fluxes**

588 River discharges are extracted from the UNH/GRDC runoff dataset (Fekete et al., 2002). These
589 discharges represent long-term averages (1960-1990) of monthly and annual runoff at 0.5 degree
590 resolution. The dataset is a composite of long-term gauging data, which provides average runoff for
591 the largest river basins, and a climate driven water balance model (Fekete et al., 2002). Total runoff
592 values are then aggregated for each watershed at the coarser 0.5 degree resolution (Fig. 3b). Next,
593 seasonal mean values (in $\text{m}^3 \text{s}^{-1}$) are derived in order to account for the intra-annual variability in
594 water fluxes. Based on annual carbon and nutrients inputs from the watersheds (Mg y^{-1}), mean
595 annual concentrations (mmol m^{-3}) are estimated for each watershed using the UNH/GRDC annual
596 runoff ($\text{km}^3 \text{y}^{-1}$). Mean seasonal concentrations are then calculated from the seasonally resolved
597 river water fluxes of a given sub-region.

599 Annual inputs of dissolved organic carbon (DOC), particulate organic carbon (POC) and inorganic
600 nutrients are derived from the globalNEWS2 model (Mayorga et al., 2010). Global NEWS is a spatially
601 explicit, multi-element (N, P, Si, C) and multi-form global model of nutrient exports by rivers. In a
602 nutshell, DOC exports are a function of runoff, wetland area, and consumptive water use (Harrison
603 et al., 2005). No distinction is made between agricultural and natural landscapes, since they appear
604 to have similar DOC export coefficients (Harrison et al., 2005). Sewage inputs of OC are ignored in
605 GlobalNEWS, because their inclusion did not improve model fit to data (Harrison et al., 2005). POC
606 exports from watersheds are estimated using an empirical relationship with Suspended Particulate
607 Matter (SPM; Ludwig et al., 1996). Inorganic nitrogen (DIN) and phosphorus (DIP) fluxes calculated
608 by GlobalNEWS depend on agriculture and tropical forest coverage, fertilizer application, animal
609 grazing, sewage input, atmospheric N deposition and biological N fixation (Mayorga et al., 2010). The
610 inputs of dissolved silica (DSi) are controlled by soil bulk density, precipitation, slope, and presence
611 of volcanic lithology (Beusen et al., 2009).

612 The DIN speciation is not provided by the GlobalNEWS2 model. The NH_4 and NO_3 concentrations are
613 therefore determined independently on the basis of an empirical relationship between ammonium
614 fraction (NH_4/DIN ratio) and DIN loads (Meybeck, 1982). Dissolved Oxygen (DO) concentrations are
615 extracted from the water quality criteria recommendations published by the United States
616 Environmental Protection Agency (EPA, 2009). The same source is used for phytoplankton
617 concentrations, using a chlorophyll-a to phytoplankton carbon ratio of $50 \text{ gC (gChla)}^{-1}$ (Riemann et
618 al., 1989) to convert the EPA values to carbon units used in the present study.

619 Inputs of dissolved inorganic carbon (DIC) and total Alkalinity (ALK) are calculated from values
620 reported in the GLORICH database (Hartmann et al., 2009). For each watershed, seasonal mean
621 values of DIC and ALK concentrations are estimated from measurements performed at the sampling
622 locations that are closest to the river-estuary boundary. The spatial distribution of annual inputs of
623 $\text{TOC}=\text{DOC}+\text{POC}$, DIC, and $\text{TC}=\text{TOC}+\text{DIC}$ from continental watersheds to estuaries are reported in Fig.

624 5a, 5c and 5d, respectively. The contribution of tidal wetlands to the TOC inputs is also shown (Fig.
 625 5b). Overall, the TC input over the entire model domain is estimated at 4.6 Tg C yr⁻¹, which falls in
 626 the lower end of previous reported estimations (Najjar et al. 2012).

627

628 2.4.3 Inputs from tidal wetlands

629 The DOC input of estuarine wetlands (Fig. 5b) scales to their fraction, *W*, of the total estuarine and is
 630 calculated using the GlobalNEWS parameterization:

$$Y_{DOC} = \frac{[(E_{C_{wet}} * W) + E_{C_{dry}} * (1 - W)] * R^a * Q_{act}}{Q_{nat}} \quad (12)$$

631

$$\frac{Y_{DOC_{wet}}}{Y_{DOC}} = \frac{E_{C_{wet}} * W}{E_{C_{wet}} * W + E_{C_{dry}} * (1 - W)} \quad (13)$$

632

633 where *Y_{DOC}* is the DOC yield (kg C km⁻² y⁻¹) calculated for the entire watershed, *Y_{DOC_{wet}}* is the
 634 estimated DOC yield from wetland areas (kg C km⁻² y⁻¹), *Q_{act}/Q_{nat}* is the ratio between the measured
 635 discharge after dam construction and before dam construction, *E_{C_{wet}}* and *E_{C_{dry}}* (kg C km⁻² y⁻¹) are
 636 the export coefficients of DOC from wetland and non-wetland soils, respectively. *W* is the
 637 percentage of the land area within a watershed that is covered by wetlands, *R* is the runoff (m y⁻¹)
 638 and *a* is a unit-less calibration coefficient defining how non-point source DOC export responds to
 639 runoff. The value of *a* is set to 0.95, consistent with the original GlobalNEWS -DOC model of Harrison
 640 et al. (2005). The carbon load *Y_{DOC_{wet}}* is then exported as a diffuse source along the relevant
 641 portions of estuary. The estuarine segments receiving carbon inputs from tidal wetlands are
 642 identified using the National Wetlands Inventory of the U.S. Fish and Wildlife Service (U.S. Fish and
 643 Wildlife Service, 2014). The inputs from those systems are then allocated to the appropriate grid cell

644 of the model domain using GIS. The flux calculated is an annual average that is subsequently
645 partitioned between the four seasons as a function of the mean seasonal temperature, assumed to
646 be the main control of the wetland-estuarine exchange. This procedure reflects the observation that
647 in spring and early summer, DOC export is small as a result of its accumulation in the salt marshes
648 induced by the high productivity (Dai and Wiegert, 1996), (Jiang et al., 2008). In late summer and fall,
649 the higher water temperature and greater availability of labile DOC contribute to higher bacterial
650 remineralization rates in the intertidal marshes (Cai et al., 1999; Middelburg et al., 1996; Wang and
651 Cai, 2004), which induce an important export. This marsh production-recycle-export pattern is
652 consistent with the observed excess DIC signal in the offshore water (Jiang et al. 2013). DIC export
653 from tidal wetlands is neglected here because it is assumed that OC is not degraded before reaching
654 the estuarine realm. Although this assumption may lead to an overestimation of OC export from
655 marshes and respiration in estuarine water, it will not significantly affect the water $p\text{CO}_2$ and
656 degassing in the estuarine waters because mixing is faster than respiration.

657 **2.4.4 Concentrations at the estuarine mouth**

658 For each estuary, the downstream boundary is located 20 km beyond the mouth to minimize the
659 bias introduced by the choice of a fixed concentration boundary condition to characterize the ocean
660 water masses (e.g. Regnier et al., 1998). This approach also reduces the influence of marine
661 boundary conditions on the simulated estuarine dynamics, especially for all organic carbon species
662 whose concentrations are fixed at zero at the marine boundary. This assumption ignores the
663 intrusion of marine organic carbon into the estuary during the tidal cycle but allows focusing on the
664 fate of terrigenous material and its transit through the estuarine filter. DIC concentrations are
665 extracted from the GLODAP dataset (Key et al., 2004), from which ALK and pH are calculated
666 assuming CO_2 equilibrium between coastal waters and the atmosphere. The equilibrium value is
667 computed using temperature (WOA2009, Locarnini et al., 2010) and salinity (WOA2009, Antonov et
668 al. (2010)) data which vary both spatially and temporally. The equilibrium approach is a reasonable

669 assumption because differences in partial pressure $\Delta p\text{CO}_2$ between coastal waters and the
 670 atmosphere are generally much smaller (0-250 μatm (Signorini et al., 2013)) than those reported for
 671 estuaries ($\Delta p\text{CO}_2$ in the range 0-10000 μatm (Borges and Abril, 2012)). Salinity, DO, NO_3 , DIP and DSI
 672 concentrations are derived from the World Ocean Atlas (Antonov et al., 2010; Garcia et al., 2010a;
 673 Garcia et al., 2010b). NH_4 concentrations are set to zero in marine waters. For all variables, seasonal
 674 means are calculated for each grid cell of the boundary.

675

676 **2.5 Biogeochemical indicators**

677 The model outputs (longitudinal profiles of concentration and reaction rates) are integrated in time
 678 over the entire volume or surface of each estuary to produce the following indicators of the
 679 estuarine biogeochemical functioning (Regnier et al., 2013b): the mean annual Net Ecosystem
 680 Metabolism (*NEM*), the air-water CO_2 flux (*FCO₂*), the carbon and nitrogen filtering capacity (*CFilt*
 681 and *NFilt*) and their corresponding element budgets. The *NEM* (molC y^{-1}) (Caffrey, 2004; Odum,
 682 1956) is defined as the difference between net primary production (*NPP*) and total heterotrophic
 683 respiration (*HR*) at the system scale:

$$NEM = \int_0^{365} \int_0^L [NPP(x, t) - R_{aer}(x, t) - R_{den}(x, t)] * B(x) * H(x, t) dx dt \quad (14)$$

684

685 where *NPP* is the Net Primary Production ($\text{mol C m}^{-3} \text{y}^{-1}$), R_{aer} the aerobic degradation of organic
 686 matter (in $\text{mol C m}^{-3} \text{y}^{-1}$) and R_{den} the denitrification (in $\text{mol C m}^{-3} \text{y}^{-1}$) (see Volta et al., 2014 for
 687 detailed formulations). *NEM* is thus controlled by the production and decomposition of
 688 autochthonous organic matter, by the amount and degradability of organic carbon delivered by
 689 rivers and tidal wetlands and by the export of terrestrial and in-situ produced organic matter to the
 690 adjacent coastal zone. Following the definition of *NEM*, the trophic status of estuaries can be net

691 heterotrophic ($NEM < 0$) when HR exceeds NPP or net autotrophic ($NEM > 0$), when NPP is larger than
 692 HR because the burial and export of autochthonous organic matter exceeds the decomposition of
 693 river-borne material.

694 The FCO_2 (mol C y^{-1}) is defined as:

$$FCO_2 = \int_0^{365} \int_0^L RCO_2(x, t) * B(x) dx dt \quad (15)$$

695

$$RCO_2(x, t) = -v_p(x, t) ([CO_2(aq)](x, t) - K_0(x, t) * P_{CO_2}(x, t)) \quad (16)$$

696

697 where RCO_2 ($\text{molC m}^{-2} \text{y}^{-1}$) is the rate of exchange in CO_2 at the air-water interface per unit surface
 698 area, v_p is the piston velocity (m y^{-1}) and is calculated according to Regnier et al. (2002) to account
 699 for the effect of current velocity and wind speed, $[CO_2(aq)]$ is the concentration of CO_2 in the
 700 estuary (mol m^{-3}), K_0 is Henry's constant of CO_2 in sea water ($\text{mol m}^{-3} \text{atm}^{-1}$) and P_{CO_2} is the
 701 atmospheric partial pressure in CO_2 (atm).

702 The carbon filtering capacity (in %) corresponds to the fraction of the river-borne supply that is lost
 703 to the atmosphere and is defined here as the ratio of the net outgassing flux of CO_2 and the total
 704 inputs of C, e.g. total carbon expressed as the sum of inorganic and organic carbon species, both in
 705 the dissolved and particulate phases.

$$CFilt = \frac{FCO_2}{\int_0^{365} Q * [TC]_{riv} dt} * 100 \quad (17)$$

707 where $[TC]_{riv}$ denote the total concentrations of C in the riverine inputs.

708 Fluxes per unit area for FCO_2 and NEM , noted $\overline{FCO_2}$ and \overline{NEM} , respectively, are defined in mol C m^{-2}
 709 y^{-1} and are calculated by dividing the integrated values calculated above by the (idealized) estuarine
 710 surface S:

711 $\overline{NEM} = \frac{NEM}{S} * 1000$ (18)

712 $\overline{FCO_2} = \frac{FCO_2}{S} * 1000$ (19)

713 Seasonal values for the biogeochemical indicators are calculated using the same formula as above,
714 but calculate the integral over a seasonal rather than annual timescale (i.e. 3 months).

715 Deleted: ¶

716 **2.6 Model-data comparison**

717 C-GEM has been specifically designed for an application on a global/regional scale requiring the
718 representation of a large number of individual and often data-poor systems. Maximum model
719 transferability and minimum validation requirements were thus central to the model design process
720 and the ability of the underlying approach in reproducing observed dynamics with minimal
721 calibration effort has been extensively tested. The performance C-GEM's one-dimensional
722 hydrodynamic and transport models using idealized geometries have been evaluated for a number
723 of estuarine systems exhibiting a wide variety of shapes (Savenije, 2012). In particular, it has been
724 shown that the estuarine salt intrusion can be successfully reproduced using the proposed modeling
725 approach (Savenije 2005; Volta et al., 2014; 2016b). In addition, C-GEM's biogeochemistry has also
726 been carefully validated for geometrically contrasting estuarine system in temperate climate zones.
727 Simulations for the Scheldt Estuary (Belgium and the Netherlands), a typical funnel-shaped estuary,
728 were validated through model-data and model-model comparison (Volta et al., 2014; Volta et al.,
729 2016a). Furthermore, simulations for the Elbe estuary (Germany), a typical prismatic shape estuary
730 that drains carbonate terrains and, thus, exhibits very high pH was validated against field data (Volta
731 et al., 2016a). In addition, C-GEM carbon budgets have been compared budget derived from
732 observations for 6 European estuaries discharging in the North Sea (Volta et al., 2016a). Although C-
733 GEM has been specifically designed and tested for the type of regional application presented here,
734 its transferability from North Sea to US East Coast estuaries was further evaluated by assessing its

736 performance in two East Coast estuaries. First, the hydrodynamic and transport model was tested
 737 for the Delaware Bay (MAR). The model was forced with the monthly, minimal and maximal
 738 observed discharge at Trenton over the period between 1912 and 1985 (UNH/GRDC Database,
 739 [GRDC, 2014](#)). Simulated salinity profiles are compared with salinity observations from January,
 740 February, May and June (the months with the highest number of data entries), which were extracted
 741 from the UNH/GRDC Database. Figure 6 shows that the model captures both the salinity intrusion
 742 length and the overall shape of the salinity profile well. In addition, the performance of the
 743 biogeochemical model and specifically its ability to reproduce pH and pCO₂ profiles was evaluated by
 744 a model-data comparison for both the Delaware Bay (MAR) in July 2003 and the Altamaha river
 745 estuary (SAR) in October 1995. Similar to Volta et al., 2016a, the test systems were chosen due to
 746 their contrasting geometries. The Delaware Bay is a marine dominated system characterized by a
 747 pronounced funnel shape, while the Altamaha River has a prismatic estuary characteristic of river
 748 dominated systems (Jiang et al., 2008). Monthly upstream boundary conditions for nutrients, as well
 749 as observed pH data and calculated pCO₂ are extracted from datasets described in (Sharp, 2010) and
 750 (Sharp et al., 2009) for the Delaware and in [Cai and Wang, \(1998\)](#), [Jiang et al., \(2008\)](#) and (Cai et al.,
 751 1998) for the Altamaha river estuary. The additional forcings and boundary conditions are set
 752 similarly to the simulation for 2000 (see Tab. 2, 3, 4, 5, 6 in SI). Figure 7 shows that measured and
 753 simulated pH values are in good agreement with observed pH and observation-derived calculations
 754 of pCO₂. In the Delaware Bay, a pH minimum is located around km 140 and is mainly caused by
 755 intense nitrification sustained by large inputs of NH₄ from the Philadelphia urban area, coupled to an
 756 intense heterotrophic activity. Both processes lead to a well-developed pCO₂ increase in this area
 757 (Fig. 7c). Overall, the longitudinal pCO₂ profile of the Delaware estuary is characterized by values
 758 close to equilibrium with the atmosphere in the widest section of the Delaware Bay (near the
 759 estuarine mouth and throughout the 40 first kilometers of the system) and values above 1200 µatm
 760 at kilometer 150 and beyond, where characteristic salinities are below 5. Although the profile
 761 presented here is simulated using boundary conditions representative of July 2003 and no pCO₂ data

Deleted: ,

Deleted: Fekete et al.

Deleted: 2000

Deleted: (

Deleted: ,

Deleted: ;

Deleted: ,

Deleted: b

Moved down [1]: Although no pCO₂ data were available for validation for the period from which boundary conditions were extracted, the simulated profile agree with pCO₂ measurement from July 2013 presented by Joesoef et al. (2015)

Formatted: Subscript

Deleted: with pCO₂

Deleted: close to

Deleted: at

Moved (insertion) [1]

779 were available for validation for this period, a recent study by Joesoef et al. (2015) reports a similar
780 longitudinal pCO₂ profile in July 2013. For the Altamaha river estuary, pH steadily increases from
781 typical river to typical coastal ocean values (Fig. 7b). In addition, both observations and model
782 results reveal that outgassing is very intense in the low-salinity region with more than a 5 fold
783 decrease in pCO₂ between salinity 0 and 5 (Fig. 7d).

Deleted: e
Deleted:
Deleted: from which boundary conditions were extracted, the simulated profile agree with pCO₂ measurement from July 2013 presented
Formatted: Subscript

784 While such local validations allow assessing the performance of the model for a specific set of
785 conditions, the purpose of this study is to capture the average biogeochemical behavior of the
786 estuaries of the eastern coast of the US. Therefore, in addition to the system-specific validation,
787 published annually averaged FCO₂ estimates for 12 tidal systems located within the study area
788 collected over the 1994-2006 period are compared to simulated FCO₂ for conditions representative
789 of the year 2000. Overall, simulated FCO₂ are comparable to values reported in the literature (Tab.

Deleted: 13

790 2). Although significant discrepancies are observed, at the level of individual systems, the model
791 captures remarkably well the overall behaviors of estuaries along the East coast of the US in term of
792 intensity of CO₂ evasion rate. The model simulates low CO₂ efflux (< 5 mol C m⁻² yr⁻¹) for the 6
793 systems where such conditions have been observed, while the 5 systems for which the CO₂ evasion
794 exceeds 10 mol C m⁻² yr⁻¹ are the same in the observations and in the model runs. The discrepancies
795 at the individual system level likely result from a combination of factors, including the choice of
796 model processes and their parametrization, the uncertainties in constraining boundary conditions
797 and the limited representability of instantaneous and local observations.

Deleted: , which sometimes can significant,
Deleted: are observed
Deleted: trend
Deleted: in
Deleted: across estuaries
Deleted: 7
Deleted: 6
Deleted: discrepancy

Deleted: observed

798 **3 Results and discussion**

799 **3.1 Spatial variability of estuarine carbon dynamics**

800 Figure 8 presents the spatial distribution of simulated mean annual $\overline{FCO_2}$ and $-\overline{NEM}$ (Fig. 8a), as well
801 as FCO_2 and $-NEM$ (Fig. 8b). In general, mean annual $\overline{FCO_2}$ are about 30% larger than mean annual
802 \overline{NEM} , with the exception of six estuaries situated in the North of the coastal segment. Overall, the

820 \overline{NEM} is characterized by smaller system to system variability compared to the $\overline{FCO_2}$ in all regions. In
821 addition, Fig. 8 reveals distinct differences across the three coastal segments and highlights the
822 important influence of the estuarine geometry and residence time, as well as the latitudinal
823 temperature gradient on estuarine carbon cycling.

824 Overall, $\overline{FCO_2}$ values are the lowest in the NAR (mean flux = $17.3 \pm 16.4 \text{ mol C m}^{-2} \text{ y}^{-1}$; surface
825 weighted average = $23.1 \text{ mol C m}^{-2} \text{ y}^{-1}$), consistent with previously reported very low values for small
826 estuaries surrounding the Gulf of Maine (Hunt et al., 2010; 2011; Tab. 2). In contrast, \overline{NEM} reveals a
827 regional minimum in the NAR ($-51.2 \pm 16.6 \text{ mol C m}^{-2} \text{ y}^{-1}$; surface weighted average = $-52.8 \text{ mol C m}^{-2}$
828 y^{-1}). The MAR is characterized by intermediate values for $\overline{FCO_2}$, with a mean flux of $26.3 \pm 34.6 \text{ mol}$
829 $\text{C m}^{-2} \text{ y}^{-1}$ (surface weighted average = $11.1 \text{ mol C m}^{-2} \text{ y}^{-1}$) and lowest values for \overline{NEM} ($-15.1 \pm 14.2 \text{ mol}$
830 $\text{C m}^{-2} \text{ y}^{-1}$; surface weighted average = $-7.4 \text{ mol C m}^{-2} \text{ y}^{-1}$). This region also shows the largest variability
831 in CO_2 outgassing compared to the NAR and SAR, with the standard deviation exceeding the mean
832 $\overline{FCO_2}$, and individual estimates ranging from $3.9 \text{ mol C m}^{-2} \text{ y}^{-1}$ to $150.8 \text{ mol C m}^{-2} \text{ y}^{-1}$. This variability
833 is mainly the result of largely variable estuarine surface areas and volumes. Some of the largest East
834 coast estuaries (e.g. Chesapeake and Delaware Bays), as well as some of smallest estuaries (e.g. York
835 River and Hudson River estuaries, Raymond et al., 1997; 2000), are located in this region (Tab. 2 and
836 4). The maximum values of $150.8 \text{ mol C m}^{-2} \text{ y}^{-1}$ simulated in the MAR are similar to the highest FCO_2
837 reported in the literature ($132.3 \text{ mol C m}^{-2} \text{ y}^{-1}$ for the Tapti estuary in India; Sarma et al., 2012). The
838 SAR is characterized by the highest mean $\overline{FCO_2}$ ($46.7 \pm 33.0 \text{ mol C m}^{-2} \text{ y}^{-1}$; surface weighted average
839 = $40.0 \text{ mol C m}^{-2} \text{ y}^{-1}$) and intermediate \overline{NEM} ($-36.8 \pm 24.7 \text{ mol C m}^{-2} \text{ y}^{-1}$; surface weighted average = -
840 $31.2 \text{ mol C m}^{-2} \text{ y}^{-1}$).

841 The NAR is characterized by a regional minimum in $\overline{FCO_2}$, and only contributes 4.6% to the total
842 FCO_2 of the East coast of the US, owing to the small cumulative surface area available for gas
843 exchange in its 10 estuarine systems. In contrast, the 18 MAR estuaries, with their large relative
844 contribution to the total regional estuarine surface area, account for as much as 70.1% of the total

845 outgassing. Because of their smaller cumulated surface area compared to those of the MAR, the 14
846 SAR estuaries account for merely 25.3% of the total outgassing despite their regional maximal $\overline{FCO_2}$.
847 A similar, yet slightly less pronounced pattern emerges for the \overline{NEM} . The NAR, MAR and SAR
848 respectively contribute 13.7%, 60.7% and 25.6% to the total regional net ecosystem metabolism. The
849 comparatively larger relative contribution of the NAR to the total NEM as compared to the total
850 FCO_2 can be explained by the importance of the specific aspect ratio for NEM . A larger ratio of
851 estuarine width b_0 and convergence length b corresponds to a more funnel shaped estuary while a
852 low ratio corresponds to a more prismatic geometry (Savenije, 2005; Volta et al., 2014). In the NAR,
853 estuaries are generally characterized by relatively narrow widths and deep-water depths, thus
854 limiting the potential surface area for gas exchange with the atmosphere. However, the relative
855 contribution of each region to the total regional NEM and FCO_2 is largely controlled by estuarine
856 surface area. Figure 9 illustrates the cumulative NEM (a) and FCO_2 (b) as a function of the cumulative
857 estuarine surface areas. The disproportionate contribution of large estuaries from the MAR
858 translates into a handful of systems (Chesapeake and Delaware Bays and the main tributaries of the
859 former, in particular) contributing to roughly half of the regional NEM and FCO_2 , in spite of relatively
860 low individual rates per unit surface area. However, the smallest systems (mostly located in the NAR
861 and SAR) nevertheless still contribute a significant fraction to the total regional NEM and FCO_2 . The
862 27 smallest systems merely account for less than 10% of the total regional estuarine surface area,
863 yet contribute 38% and 29% to the total regional NEM and FCO_2 , respectively (Fig. 9). This
864 disproportioned contribution can be mainly attributed to their high individual $\overline{FCO_2}$ and \overline{NEM} . This
865 is illustrated by the average simulated $\overline{FCO_2}$ for all 27 smallest systems (calculated as the sum of
866 each estuarine CO_2 outgassing per unit surface area divided by the total number of estuarine
867 systems) which is significantly higher ($30.2 \text{ mol C m}^{-2} \text{ y}^{-1}$) than its surface weighted average (14 mol C
868 $\text{m}^{-2} \text{ y}^{-1}$). Thereby accounting for the disproportionate contribution of very large systems (calculated
869 as the sum of each estuarine CO_2 outgassing divided by the total estuarine surface area across the
870 region).

Deleted: b0

Deleted: 2000

873 | Following the approach used in Regnier et al. (2013**b**), the contribution of each biogeochemical
874 | process to FCO_2 is assessed by evaluating their individual contribution to DIC and ALK changes taking
875 | into account the local buffering capacity of an ionic solution when TA and DIC are changing due to
876 | internal processes, but ignoring advection and mixing (Zeebe and Wolf-Gladrow 2001). In the
877 | present study, we quantify the effect of the NEM on the CO_2 balance, which is almost exclusively
878 | controlled by aerobic degradation rates because the contributions of denitrification and NPP to the
879 | net ecosystem balance are small. Nitrification, a process triggered by the transport and/or
880 | production of NH_4 in oxygenated waters, favors outgassing through its effect on pH, which shifts the
881 | acid-base equilibrium of carbonate species and increases the CO_2 concentration. The contribution of
882 | supersaturated riverine waters to the overall estuarine CO_2 dynamics is calculated as difference
883 | between all the other processes creating or consuming CO_2 . Figure 10a presents the contribution of
884 | the annually integrated *NEM*, nitrification and evasion of supersaturated, DIC enriched riverine
885 | waters to the total outgassing for each system, as well as for individual regions of the domain. The
886 | calculation of these annual values is based on the sum of the seasonal fluxes. Model results reveal
887 | that, regionally, the *NEM* supports about 50% of the estuarine CO_2 outgassing, while nitrification and
888 | riverine DIC inputs sustain about 17% and 33% of the CO_2 emissions, respectively. The relative
889 | significance of the three processes described above shows important spatial variability. In the NAR,
890 | oversaturated riverine waters and *NEM* respectively sustain 50% and 44% of the outgassing within
891 | the sub-region, while nitrification is of minor importance (6%). In the MAR, the contribution of
892 | riverine DIC inputs is significantly lower (~30%) and the main contribution to the outgassing is *NEM*
893 | (~50%); nitrification accounting for slightly less than 20% of the outgassing. In the SAR, the riverine
894 | contribution is even lower (~20%), and the outgassing is mainly attributed to the *NEM* (~55%) and
895 | nitrification (~25%). Therefore, although the model results reveal significant variability across
896 | individual systems, a clear latitudinal trend in the contribution to the total FCO_2 emerge from the
897 | analysis; the importance of oversaturated riverine water decreasing from North to South, while *NEM*
898 | and nitrification increase along the same latitudinal gradient. The increasing relative importance of

899 estuarine biogeochemical processes over riverine DIC inputs as drivers of FCO_2 along the North-
900 South gradient is largely driven by increasing temperatures from North to South, especially in the
901 SAR region (Tab. SI 1).

902 Contrasting patterns across the 3 regions can also be observed with respect to carbon filtering
903 capacities, $CFilt$ (Fig. 10b). In the NAR, over 90% of the riverine carbon flux is exported to the coastal
904 ocean. However, in the MAR, the high efficiency of the largest systems in processing organic carbon
905 results in a regional $CFilt$ that exceeds 50%. This contrast between the NAR and the MAR and its
906 potential implication for the carbon dynamics of the adjacent continental shelf waters has already
907 been discussed by Laruelle et al. (2015). In the NAR, short estuarine residence results in a much
908 lower removal of riverine carbon by degassing compared to the MAR. Laruelle et al. (2015)
909 suggested that this process could contribute to the weaker continental shelf carbon sink adjacent to
910 the NAR, compared to the MAR. In the SAR, most estuaries remove between 40% and 65% of the
911 carbon inputs. The high temperatures observed and resulting accelerated biogeochemical process
912 rates in this region favor the degradation of organic matter and contribute to increase the estuarine
913 filtering capacity for carbon. However, in the SAR, a large fraction of the OC loads is derived from
914 adjacent salt marshes located along the estuarine salinity gradients, thereby reducing the overall
915 residence time of OC within the systems. The filtering capacity of the riverine OC alone, which
916 transits through the entire estuary, would thus be higher than the one calculated here. As a
917 consequence, highest C retention rates are expected in warm tidal estuaries devoid of salt marshes
918 or mangroves (Cai, 2011).

919 **3.2 Seasonal variability of estuarine carbon dynamics**

920 Carbon dynamics in estuaries of the US East coast not only show a marked spatial variability, but also
921 vary on the seasonal timescale. Table 5 presents the seasonal distribution of NEM and FCO_2 for each
922 sub-region. In the NAR, a strong seasonality is simulated for the NEM and the summer period
923 contributes more than a third to the annually integrated value. The outgassing reveals a lower

924 seasonal variability and is only slightly higher than summer outgassing during fall and lower during
925 spring. In the MAR, summer contributes more to the *NEM* (>28% of the yearly total) than any other
926 season, but seasonality is less pronounced than in the NAR. Here, *FCO₂* is largest in winter and
927 particularly low during summer. In the SAR, summer accounts for 30 % of the *NEM*, while spring
928 contributes 21 %. *FCO₂* is relatively constant throughout the year suggesting that seasonal variations
929 in carbon processing decrease towards the lower latitudes in the SAR. This is partly related to the
930 low variability in river discharge throughout the year in lower latitudes (Tab. SI1). In riverine
931 dominated systems with low residence times, such as, for instance, the Altamaha River estuary, the
932 *CO₂* exchange at the air-water interface is mainly controlled by the river discharge because the time
933 required to degrade the entire riverine organic matter flux exceeds the transit time of OC through
934 the estuary. Therefore, the riverine sustained outgassing is highest during the spring peak discharge
935 periods. In contrast, the seasonal variability in *FCO₂* in long-residence, marine-dominated systems
936 with large marsh areas (e.g. Sapelo and Doboy Sound) is essentially controlled by seasonal
937 temperature variations. Its maximum is reached during summer when marsh plants are dying and
938 decomposing, as opposed to spring when marshes are in their productive stage (Jiang et al., 2008).
939 These contrasting seasonal trends have already been reported for different estuarine systems in
940 Georgia, such as the Altamaha Sound, the Sapelo Sound and the Doboy Sound (Cai, 2011). At the
941 scale of the entire East coast of the US, the seasonal trends in *NEM* reveal a clear maximum in
942 summer and minimal values during autumn and winter. The seasonality of *FCO₂* is much less
943 pronounced because the outgassing of oversaturated riverine waters throughout the year
944 contributes to a large fraction of the *FCO₂* and dampens the effect of the temperature dependent
945 processes (*NEM* and denitrification). In our simulations, the competition between temperature and
946 river discharge is the main driver of the seasonal estuarine carbon dynamics is. When discharge
947 increases, the carbon loads increase proportionally and the residence time within the system
948 decreases, consequently limiting an efficient degradation of organic carbon input fluxes. In warm

949 regions like the SAR, the temperature is sufficiently high all year round to sustain high C processing
950 rates and this explains the reduced seasonal variability in NEM.

951

952 3.3 Regional carbon budget: a comparative analysis

953 The annual carbon budget for the entire East coast of the US is summarized in Fig. 11a. The total
954 carbon input to estuaries along the East coast of the US is 4.6 Tg C y^{-1} , of which 42% arrives in
955 organic form and 58% in inorganic form. Of this total input, saltmarshes contribute 0.6 Tg C yr^{-1} ,
956 which corresponds to about 14% of the total carbon loads and 32% of the organic loads in the
957 region. The relative contribution of the saltmarshes to the total carbon input increases towards low
958 latitudes and is as high as 60% in the SAR region. Model results suggest that 2.7 Tg C y^{-1} is exported
959 to the continental shelf (25% as TOC and 75% as DIC), while 1.9 Tg C y^{-1} is emitted to the
960 atmosphere. The overall carbon filtering capacity of the region thus equals 41% of the total carbon

961 entering the [42](#) estuarine systems (river + saltmarshes). Because of the current lack of a benthic
962 module in C-GEM, the water column carbon removal occurs entirely in the form of CO_2 outgassing
963 and does not account for the potential contribution of carbon burial in sediments. The estimated
964 estuarine carbon retention presented here is thus likely a lower bound estimate. Reported to the
965 modeled surface area of the region, the total FCO_2 of 1.9 Tg C y^{-1} translates into a mean air water
966 CO_2 flux of about 14 mol C $\text{m}^{-2} \text{y}^{-1}$. This value is slightly higher than the estimate of 10.8 mol C $\text{m}^{-2} \text{y}^{-1}$
967 calculated by Laruelle et al., (2013) on the basis of local $\overline{FCO_2}$ estimates assumed to be
968 representative of yearly averaged conditions (see section 2.1). The latter was calculated as the
969 average of 13 annual $\overline{FCO_2}$ values reported in the literature (Tab. 2), irrespective of the size of the
970 systems. This approach is useful and widely used to derive regional and global carbon budgets
971 (Borges et al., 2005; Laruelle et al., 2010; Chen et al., 2013). However, it may lead to potentially
972 significant errors (Volta et al., 2016a) due to the uncertainty introduced by the spatial interpolation

Deleted: 43

974 of local measurements to large regional surface areas, while useful and widely used to derive
975 regional and global carbon budgets.

976 Regional C budgets are sparse. To our knowledge, the only other published regional assessment of
977 the estuarine carbon and CO₂ dynamics comes from a relatively well studied region: the estuaries
978 flowing into the North Sea in Western Europe (Fig. 11b). This budget was calculated using a similar
979 approach (Volta 2016a) and thus provides an ideal opportunity for a comparative assessment of C
980 cycling in these regions. However, it is important to note that there are also important differences in
981 the applied model approaches and those differences should be taken into account when comparing
982 the derived budgets. In particular, the NW European study is based on a simulation of the 6 largest
983 systems only (Elbe, Scheldt, Thames, Ems, Humber and Weser), accounting for about 40% for the
984 riverine carbon loads of the region. It assumes that the intensity of carbon processing and evasion in
985 all other smaller estuaries discharging into the North Sea (16 % of the carbon loads) can be
986 represented by the average of the 6 largest system simulation results. In addition, the Rhine-Meuse
987 system, which alone accounts for 44% of the carbon riverine inputs of the region, was treated as a
988 passive conduit with respect to carbon due to its very short freshwater residence time (Abril et al.,
989 2002). The contribution of saltmarshes to the regional carbon budget was also ignored because their
990 total surface area is much smaller than along the US East coast (Regnier et al., 2013b). Another
991 important difference is the inclusion of seasonality in the present study while the budget calculated
992 for the North Sea is derived from yearly average conditions (Volta et al., 2016a).

993 Overall, although both regions receive similar amounts of C from rivers (4.6 Tg C y⁻¹ and 5.9 Tg C y⁻¹
994 for the East coast of the US and the North Sea, respectively), they reveal significantly different C
995 filtering capacities. While the estuaries of the East coast of the US filter 41% of the riverine TC loads,
996 those from the North Sea only remove 8% of the terrestrial-derived material. This is partly due to the
997 large amounts of carbon transiting through the 'passive' Rhine-Meuse system. The regional filtering
998 capacity is higher (15%) when this system is excluded from the analysis. However, even when

999 neglecting this system, significant differences in filtering efficiencies between both regions remain.
1000 FCO_2 from the North Sea estuaries (0.5 Tg C y^{-1}) is significantly lower than the 1.9 Tg C y^{-1} computed
1001 for the East coast of the US. The reason for the lower evasion rate in NW European estuaries is
1002 essentially twofold. First, the total cumulative surface area available for gas exchange is significantly
1003 lower along the North Sea, in spite of comparable flux densities calculated using the entire estuarine
1004 surface areas of both regions ($14 \text{ mol C m}^{-2} \text{ y}^{-1}$ and $23 \text{ mol C m}^{-2} \text{ y}^{-1}$ for the East coast of the US and
1005 the North Sea, respectively). Second, although the overall riverine carbon loads are comparable in
1006 both regions (Fig. 11), the ratio of organic to inorganic matter input is much lower in the North Sea
1007 area because of the regional lithology is dominated by carbonate rocks and mixed sediments that
1008 contain carbonates (Dürr et al., 2005; Hartmann et al., 2012). As a consequence, TOC represents less
1009 than 20% of the riverine loads and only 10% of the carbon exported to the North Sea. In both
1010 regions, however, the increase of the inorganic to organic carbon ratio between input and output is
1011 sustained by a negative NEM (Fig. 11). Although the ratios themselves may significantly vary from a
1012 region of the world to the other as evidenced by these two studies, a NEM driven increase of the
1013 inorganic fraction within carbon load along the estuarine axis is consistent with the global estuarine
1014 carbon budget proposed by Bauer et al. (2013). In the East coast of the US, the respiration of riverine
1015 OC within the estuarine filter is partly compensated by OC inputs from marshes and mangroves in
1016 such a way that the input and export IC/OC ratios are closer than in the North Sea region.

1017 **3.4 Scope of applicability and model limitations**

1018 Complex multidimensional models are now increasingly applied to quantitatively explore carbon and
1019 nutrient dynamics along the land-ocean transition zone over seasonal and even annual timescales
1020 (Garnier et al., 2001; Arndt et al., 2007, 2009; Arndt and Regnier, 2007; Mateus et al., 2012).
1021 However, the application of such complex models remains limited to individual, well-constrained
1022 systems due their high data requirements and computational demand resulting from the need to
1023 resolve important physical, biogeochemical and geological processes on relevant temporal and

1024 spatial scales. The one-dimensional, computationally efficient model C-GEM has been specifically
1025 designed to reduce data requirements and computational demand and to enable regional/global
1026 scale applications (Volta et al., 2014, 2016a). However, such a low data demand and computational
1027 efficiency inevitably requires simplification. The following paragraphs critically discuss these
1028 simplifications and their implications.

1029 *Spatial resolution*

1030 Here, C-GEM is used with a 0.5° spatial resolution. While this resolution captures the features of
1031 large systems, it is still very coarse for relatively small watersheds, such as those of the St. Francis
1032 River, Piscataqua River, May River or the Sapelo River. For instance, the 5 estuaries reported by Hunt
1033 et al. (2010, 2011, see section 2.6) are all small systems covered by the same watershed at a 0.5°
1034 resolution. Only watersheds whose area spans several grid cells can be properly identified and
1035 represented (i.e. Merrimack or Penobscot with 6 and 9 cells, respectively).

Deleted: contained

1036

1037 *Hydrodynamic and Transport Model*

1038 C-GEM is based on a theoretical framework that uses idealized geometries and significantly reduces
1039 data requirements. These idealized geometries are fully described by three, easily obtainable
1040 geometrical parameters (B, b_0 , H). The model thus approximates the variability of estuarine width
1041 and cross-section along the longitudinal axis through a set of exponential functions. A
1042 comprehensive sensitivity study (Volta et al., 2014) has shown that integrated process rates are
1043 generally sensitive to changes in these geometrical parameters because of their control on estuarine
1044 residence times. For instance, Volta et al. (2014) demonstrated that the NEM, is particularly sensitive
1045 to the convergence length. Similarly, the use of constant depth profile may lead to variations of
1046 about 10% in NEM (Volta et al., 2014). Nevertheless, geometrical parameters are generally easy to
1047 constrain, especially well-monitored regions such as the US east coast. Here, all geometrical
1048 parameters are constrained on the basis of observed estuarine surface areas and average water

Deleted: b_0

Formatted: Not Superscript/ Subscript

1051 depths. In addition, the model also accounts for the slope of the estuarine channel. This approach
1052 ensures that simulated estuarine surface areas, volumes and, thus, residence times are in good
1053 agreement with those of the real systems and minimizes uncertainties associated to the physical set-
1054 up.

1055 In addition, the one-dimensional representation of the idealized estuarine systems does not resolve
1056 two- or three-dimensional circulation features induced by complex topography and density driven
1057 circulation. While C-GEM performs well in representing the dominant longitudinal gradients, its
1058 applicability to branched systems or those with aspect ratios for which a dominant axis is difficult to
1059 identify (e.g. Blackwater estuary, UK; Pearl River estuary, China; Tagus estuary, Portugal; Bay of
1060 Brest, France) is limited.

1061 *Biogeochemical Model*

1062 Although the reaction network of C-GEM accounts for all processes that control estuarine FCO_2
1063 (Borges and Abril, 2012; Cai, 2011), several, potentially important processes, such as benthic-pelagic
1064 exchange processes, phosphorous sorption/desorption and mineral precipitation, a more complex
1065 representation of the local phytoplankton community, grazing by higher trophic levels, or multiple
1066 reactive organic carbon pools are not included. Although these processes are difficult to constrain
1067 and their importance for FCO_2 is uncertain, the lack of their explicit representations induces
1068 uncertainties in C_{filt} . In particular, the exclusion of benthic processes such as organic matter
1069 degradation and burial in estuarine sediments could result in an underestimation of C_{filt} . However,
1070 because very little is known on the long term fate of organic carbon in estuarine sediments, setting
1071 up and calibrating a benthic module proves a difficult task. Furthermore, to a certain degree model
1072 parameters (such as organic matter degradation and denitrification rate constant) implicitly account
1073 for benthic dynamics. We nonetheless acknowledge that, by ignoring benthic processes and burial in
1074 particular, our estimates for the estuarine carbon filtering may be underestimated, particularly in
1075 the shallow systems of the SAR.

1076 Biogeochemical model parameters for regional and global applications are notoriously difficult to
1077 constrain (Volta et al., 2016b). Model parameters implicitly account for processes that are not
1078 explicitly resolved and their transferability between systems is thus limited. In addition, published
1079 parameter values are generally biased towards temperate regions in industrialized countries (Volta
1080 et al., 2016b). A first order estimation of the parameter uncertainty associated to the estuarine
1081 carbon removal efficiency (C_{filt}) can be extrapolated from the extensive parameter sensitivity
1082 analyses carried out by Volta et al. (2014, 2016b). These comprehensive sensitivity studies on end-
1083 member systems have shown that the relative variation in C_{filt} when a number of key
1084 biogeochemical parameters are varied by two orders of magnitude varies by $\pm 15\%$ in prismatic
1085 (short residence time on order of days) to $\pm 25\%$ in funnel-shaped (long residence time) systems.
1086 Thus, assuming that uncertainty increases linearly between those bounds as a function of residence
1087 time, an uncertainty estimate can be obtained for each of our modelled estuary. With this simple
1088 method, the simulated regional C_{filt} of 1.9 Tg C yr⁻¹ would be associated with an uncertainty range
1089 comprised between 1.5 and 2.2 Tg C yr⁻¹. Our regional estuarine CO₂ evasion estimate is thus
1090 reported with moderate confidence. Furthermore, in the future, this uncertainty range could be
1091 further constrained using statistical methods such as Monte Carlo simulations (e.g. Lauerwald et al.,
1092 2015).

Deleted: is

1093 *Boundary Conditions and Forcings*

1094 In addition, simulations are only performed for climatological means over the period 1990-2010
1095 without resolving interannual and secular variability. Boundary conditions and forcings are critical as
1096 they place the modelled system in its environmental context and drive transient dynamics. However,
1097 for regional applications, temporally resolved boundary conditions and forcings are difficult to
1098 constrain. C-GEM places the lower boundary condition 20 km from the estuarine mouth into the
1099 coastal ocean and the influence of this boundary condition on simulated biogeochemical dynamics is
1100 thus limited. At the lower boundary condition, direct observations for nutrients and oxygen are

1102 | extracted from databases such as the World Ocean Atlas (Antonov et al., 2010). However, lower
1103 | boundary conditions for OC and pCO₂ (zero concentration for OC and assumption of pCO₂
1104 | equilibrium at the sea side) are simplified. This approach does not allow addressing the additional
1105 | complexity introduced by biogeochemical dynamics in the estuarine plume (see Arndt et al., 2011).
1106 | Yet, these dynamics only play a secondary role in the presented study that focuses on the role of the
1107 | estuarine transition zone in processing terrestrial-derived carbon.

Deleted: 4

1108 | Constraining upper boundary conditions and forcings is thus more critical. Here, C-GEM is forced by
1109 | seasonally-averaged conditions for Q, T, and radiation. To date, GlobalNEWS only provide yearly-
1110 | averaged conditions for a number of upper boundary conditions (Seitzinger et al., 2005; Mayorga et
1111 | al., 2010), representative of the year 2000. Simulations are thus only partly transient (induced by
1112 | seasonality in Q, T and radiation) and do not resolve short-lived events such as storms or extreme
1113 | drought conditions. In addition, direct observations of upper boundary conditions are rarely

1114 | available, in particular over seasonal or annual timescales. For the US East Coast estuaries, direct
1115 | observations are only available for O₂, Chlorophyll-a, DIC and Alk. For DIC and alkalinity boundary
1116 | conditions are constrained by calculating the average concentration over a period of about three
1117 | decades. In addition, observational data are extracted at the station closest to the model's upper
1118 | boundary, which might be still located several kilometres upstream or downstream of the model
1119 | boundary. Upper boundary conditions of POC, DOC, DIN, DIP, DSi are extracted from GlobalNews
1120 | and thus model-derived. As a consequence, our results are thus intimately dependent on the
1121 | robustness of the GlobalNEWS predictions. These values are usually only considered robust
1122 | estimates for watersheds larger than ~10 cells (Beusen et al., 2005), which only correspond to 13 of
1123 | the 42 estuaries modelled in this study.

Deleted: -

Deleted: chlorophyll

Deleted: and

Deleted: is

Deleted: 43

1124 | *Model-data comparison*

1125 | The generic nature of the applied model approach renders a direct validation of model results on the
1126 | basis of local and instantaneous observational data (e.g. longitudinal profiles) difficult. In particular

Deleted: and, i

1134 the applications of seasonally/annually averaged or model-deduced boundary conditions, which are
1135 likely not representative of these long-term average conditions, do not lend themselves well to
1136 comparison with punctual measurements. Therefore, model performance is evaluated on the basis
1137 of spatially aggregated estimates (e.g. regional FCO_2 estimates based on local measurements) rather
1138 than system-to-system comparisons with longitudinal profile from specific days. However, note that
1139 the performance of C-GEM has been intensively tested by specific model-data comparisons for a
1140 number of different systems (e.g. Volta et al., 2014, 2016a) and we are thus confident of its
1141 predictive capabilities.

Deleted: application

Deleted: renders a direct validation of model results on the basis of local and instantaneous observational data (e.g. longitudinal profiles),

Deleted: is

Deleted: , difficult

1142 Despite the numerous simplifying assumptions inevitably required for such a regional assessment of
1143 carbon fluxes along the land-ocean continuum, the presented approach does nevertheless provide
1144 an important step forward in evaluating the role of land-ocean transition systems in the global
1145 carbon cycle. It provides a first robust estimate of carbon dynamics based on a theoretically well-
1146 founded and carefully tested, spatially and temporally resolved model approach. This approach
1147 provides novel insights that go beyond those gained through traditionally applied zero-salinity
1148 method or box model approaches. In addition, it also highlights critical variables and data gaps and
1149 thus helps guide efficient monitoring strategies.

1150 **3.5 Towards predictors of the estuarine carbon processing**

1151 The mutual dependence between geometry and transport in tidal estuaries and, ultimately, their
1152 biogeochemical functioning (Savenije, 1992; Volta et al., 2014) allows relating easily extractable
1153 parameters linked to their shape or their hydraulic properties to biogeochemical indicators. In this
1154 section, we explore the relationships between such simple physical parameters and indicators of the
1155 estuarine carbon processing \overline{NEM} , $\overline{FCO_2}$ and $CFlit$. In order to account for the effect of temperature
1156 on C dynamics, \overline{NEM} and $\overline{FCO_2}$ are also normalized to the same temperature (arbitrarily chosen to
1157 be 0 degree). These normalized values are obtained by dividing \overline{NEM} and $\overline{FCO_2}$ by a Q_{10} function
1158 $f(T)$ (see Volta et al., 2014). This procedure allows accounting for the exponential increase in the rate

1166 of several temperature dependent processes contributing to the NEM (i.e. photosynthesis, organic
1167 carbon degradation...). Applying the same normalization to $-\overline{NEM}$ and $\overline{FCO_2}$ is a way of testing how
1168 intimately linked NEM and FCO_2 are in estuarine systems. Indeed linear relationships relating one to
1169 the other have been reported (Mayer and Eyre, 2012). The three indicators are then investigated as
1170 a function of the ratio between the estuarine surface S and the seasonal river discharge Q . The
1171 surface area is calculated from the estuarine width and length, as described by equation 2, in order
1172 to use a parameter which is potentially applicable to other regions for which direct estimates of the
1173 real estuarine surface area is not available. Since the fresh water residence time of a system is
1174 obtained by dividing volume by river discharge, the S/Q ratio is also intimately linked to residence
1175 time. Here, we choose to exclude the estuarine depth from the analysis because this variable cannot
1176 be easily quantified from maps or remote sensing images and would thus compromise the
1177 applicability of a predictive relationship on the global scale. However, from dimensional analysis, S/Q
1178 can be viewed as a water residence time normalized to meter depth of water. As shown by equation
1179 3, S only requires constraining $B0$ and width convergence length b , two parameters that can readily
1180 be extracted from the Google Earth engine. Global database of river discharges, as for instance
1181 RivDIS (Vörösmarty et al., 1996) are also available in such a way that the S/Q ratio can potentially be
1182 extracted for all estuaries around the globe.

1183 Figure 12a reveals that small values of S/Q are associated with the most negative $\overline{NEM} / f(T)$. The
1184 magnitude of the \overline{NEM} then exponentially decreases with increasing values of S/Q . Estuaries
1185 characterized by small values of S/Q are mainly located in the NAR sub-region and correspond to
1186 small surface area, and thus short residence time systems. It is possible to quantitatively relate -
1187 $\overline{NEM} / f(T)$ and S/Q through a power law function ($y = 25.85 x^{-0.64}$ with a $r^2 = 0.82$). The coefficient
1188 of determination remains the same when excluding estuaries from the NAR region and the equation
1189 itself is not significantly different, although those estuaries on their own do not display any
1190 statistically significant trend (Tab. 6). The decrease in the intensity of the net ecosystem metabolism

1191 in larger estuaries (Fig 8), characterized by high S/Q ratios, can be related to the extensive
1192 consumption of the organic matter pool during its transit through the estuarine filter. However,
1193 when reported to the entire surface area of the estuary, larger systems (with high values of S/Q) still
1194 reveal the most negative surface integrated *NEM* (Fig. 12b). It can also be noted that some estuaries
1195 from the NAR region display very low values of $-NEM$. These data points correspond to fall and
1196 winter simulations for which the temperature was relatively cold (<5 °C) and biogeochemical
1197 processing was very low.

1198 The overall response of $\overline{FCO_2}/f(T)$ to S/Q is comparable to that of $-\overline{NEM}/f(T)$ (Fig. 12c), with
1199 lower values of $\overline{FCO_2}$ observed for high values of S/Q. However, for $S/Q < 3 \text{ days m}^{-1}$, the $\overline{FCO_2}$
1200 values are very heterogeneous and contain many, low $\overline{FCO_2}$ outliers from the NAR region. These
1201 data points generally correspond to low water temperature conditions which keep pCO₂ low, even if
1202 the system generates enough CO₂ internally via *NEM*. Thus, the well-documented correlation
1203 between \overline{NEM} and $\overline{FCO_2}$ (Maher and Eyre, 2012) does not seem to hold for systems with very short
1204 residence times. For systems with $S/Q > 3 \text{ days m}^{-1}$, we obtain a regression $FCO_2 = -0.64 \times NEM + 5.96$
1205 with a r^2 of 0.46, which compares well with the relation $FCO_2 = -0.42 \times NEM + 12$ proposed by Maher
1206 and Eyre (2012) who used 24 seasonal estimates from small Australian estuaries. However, our
1207 results suggest that this relationship cannot be extrapolated to small systems such as those located
1208 in the NAR. Figure 12d, which reports non-normalized FCO_2 reveals a monotonous increase of FCO_2
1209 with S/Q. This suggests that, unlike the *NEM* for which the normalization by a temperature function
1210 allowed explaining most of the variability; FCO_2 is mostly controlled by the water residence time
1211 within the system. Discharge is the main FCO_2 driver in riverine dominated systems, while
1212 interactions with marshes are driving the outgassing in marine dominated systems surrounded by
1213 marshes. Net aquatic biological production (*NEM* being negative or near 0) in large estuaries (with
1214 large S/Q) is another important reason for low FCO_2 in such systems. For example, despite the higher
1215 CO₂ degassing flux in the upper estuary of the Delaware, strong biological CO₂ uptake in the mid-bay

1216 and near zero NEM in the lower bay result in a much lower FCO_2 for the entire estuary (Joesoef et al.
1217 2015). In systems with $S/Q < 3 \text{ days m}^{-1}$, the short residence time prevents the excess CO_2 of
1218 oversaturated water from being entirely exchanged with the atmosphere and simulations reveal that
1219 the estuarine waters are still oversaturated in CO_2 at the estuarine mouth. Thus, the inorganic
1220 carbon, produced by the decomposition of organic matter, is not outgassed within the estuary but
1221 exported to the adjacent continental shelf waters. This result is consistent with the observation-
1222 based hypothesis of Laruelle et al. (2015) for the NAR estuaries. As a consequence of the distinct
1223 behavior of short residence time systems, the coefficient of determination of the best-fitted power
1224 law function relating $\overline{FCO_2}$ and S/Q is only significant if NAR systems are excluded ($y = 31.64 x^{-0.58}$
1225 with a $r^2 = 0.70$). This thus suggests that such relationships (as well as that proposed by Maher and
1226 Eyre, 2012) cannot be applied to any system but only those for which $S/Q > 3 \text{ day m}^{-1}$.

1227 Finally, Fig. 12e reports the simulated mean seasonal carbon filtering capacities as a function of the
1228 depth normalized residence time. Not surprisingly, and in overall agreement with previous studies
1229 on nutrient dynamics in estuaries (Nixon et al., 1996), the carbon filtering capacity increases with
1230 S/Q . The best statistical relation between $CFilt$ and S/Q is obtained when including all 3 regions,
1231 resulting in $r^2 = 0.70$ ($y = 40.64 \log_{10}(x) + 11.84$). Very little C removal occurs in systems with $S/Q < 1$
1232 day m^{-1} . For systems characterized by longer depth-normalized residence times, $CFilt$ increases
1233 regularly, and reaches 100% for $S/Q > 100 \text{ day m}^{-1}$. Such high values are only observed for very large
1234 estuaries from the MAR region (Delaware and Chesapeake Bays); the majority of our systems had an
1235 S/Q range between 1 and 100 day m^{-1} . The quantitative assessment of estuarine filtering capacities
1236 is further complicated by the complex interplay of estuarine and coastal processes. Episodically,
1237 marked spatial variability in concentration gradients near the estuarine mouth may lead to a reversal
1238 of net material fluxes from coastal waters into the estuary (Regnier et al., 1998; Arndt et al. 2011).
1239 Our results show that this feature is particularly significant for estuaries with a large width at the
1240 mouth and short convergence length (funnel shaped or 'Bay type' systems). These coastal nutrient
1241 and carbon inputs influence the internal estuarine C dynamics and lead to filtering capacities that

1242 can exceed 100%. This feature is particularly significant in summer, when riverine inputs are low and
1243 the marine material is intensively processed inside the estuary.

1244 Previous work investigated the relationship between fresh water residence time and nutrient
1245 retention (Nixon et al., 1996; Arndt et al., 2011; Laruelle, 2009). These studies, however, were
1246 constrained by the scarcity of data. For instance, the pioneering work of Nixon et al. (1996) only
1247 relied on a very limited number (<10) of quite heterogeneous coastal systems, all located along the
1248 North Atlantic. Here, our modeling approach allows us to generate 168 (42 x 4) data points, each
1249 representing a system-scale biogeochemical behavior. Together, this database spans the entire
1250 spectrum of estuarine settings and climatic conditions found along the East coast of the US. In
1251 addition, the ratio S/Q used as master variable for predicting temperature normalized $-\overline{NEM}$, $\overline{FCO_2}$
1252 and $CFilt$ only requires a few easily accessible geometric parameters (B_0 , b and L) and an estimate of
1253 the river discharge. While it is difficult to accurately predict $\overline{FCO_2}$ for small systems such as those
1254 located in the NAR region, the relationships found are quite robust for systems in which $S/Q > 3$ days
1255 m^{-1} . Most interestingly, $CFilt$ values reveal a significant correlation with S/Q and could be used in
1256 combination with global riverine carbon delivery estimates such as GlobalNews 2 (Mayorga et al.,
1257 2010) to constrain the estuarine CO_2 evasion and the carbon export to the coastal ocean at the
1258 continental and global scales.

1259 4. Conclusions

1260 This study presents the first complete estuarine carbon budget for the East coast of the US using a
1261 modeling approach. The structure of the model C-GEM relies on a restricted number of readily
1262 available global datasets to constrain boundary conditions and limits the number of geometrical and
1263 physical parameters to be constrained. Our simulations predict a total CO_2 outgassing of $1.9 \text{ Tg C } \gamma^{-1}$
1264 for all tidal estuaries of the East coast of the US. This quantification accounts for the seasonality in
1265 estuarine carbon processing as well as for distinct individual behaviors among estuarine types
1266 (marine or river dominated). The total carbon output to the coastal ocean is estimated at $2.7 \text{ TgC } \gamma^{-1}$,

Deleted: 172

Deleted: 43

1269 and the carbon filtering capacity with respect to riverine, marshes and mangrove inputs is thus on
1270 the order of 40%. This value is significantly higher than the recently estimated C filtering capacity for
1271 estuaries surrounding the North Sea using a similar approach (Volta et al., 2016a), mainly because
1272 the surface area available for gas exchange and the draining lithology limits the CO₂ evasion in the
1273 NW European systems. At the regional scale of the US East coast estuaries, net heterotrophy is the
1274 main driver (50%) of the CO₂ outgassing, followed by the ventilation of riverine supersaturated
1275 waters entering the estuarine systems (32%) and nitrification (18%). The dominant mechanisms for
1276 the gas exchange and the resulting carbon filtering capacities nevertheless reveal a clear latitudinal
1277 pattern, which reflects the shapes of estuarine systems, climatic conditions and dominant land-use
1278 characteristics.

1279 Our model results are used to derive predictive relationships relating the intensity of the area-based
1280 Net Ecosystem Metabolism (\overline{NEM}), air-water CO₂ exchange ($\overline{FCO_2}$) and the carbon filtering capacity
1281 ($CFilt$) to the depth normalized residence time, expressed as the ratio of the estuarine surface area
1282 to the river discharge. In the future, such simple relationships relying on readily available geometric
1283 and hydraulic parameters could be used to quantify carbon processing in areas of the world devoid
1284 of direct measurements. However, it is important to note that such simple relationships are only
1285 valid over the range of boundary conditions and forcings explored and may not be applicable to
1286 conditions that fall outside of this range. In regions with better data coverage, such as the one
1287 investigated here, our study highlights that the regional-scale quantification, attribution, and
1288 projection of estuarine biogeochemical cycling are now at reach.

1289 **5. Acknowledgements**

1290 G. G. Laruelle is Chargé de recherches du F.R.S.-FNRS at the Université Libre de Bruxelles. The
1291 research leading to these results has received funding from the European Union's Horizon 2020
1292 research and innovation programme under the Marie Skłodowska-Curie grant agreement No 643052

1293 (C-CASCADES project). The authors thank V. L. Mulder for her thorough reading of the manuscript
1294 upon submission.

1295

1296 **References:**

- 1297 Abril, G., Nogueira, M., Etcheber, H., Cabeçadas, G., Lemaire, E., and Brogueira, M.J.: Behaviour of
1298 organic carbon in nine contrasting European estuaries. *Estuar. Coast. Shelf Sci.*, 54, 241-262,
1299 2002.
- 1300 Antonov, J.I., Seidov, D., Boyer, T.P., Locarnini, R.A., Mishonov, A.V., Garcia, H.E., Baranova, O.K.,
1301 Zweng, M.M., and Johnson, D.R.: *World Ocean Atlas 2009, Volume 2: Salinity*. S., 2010.
- 1302 Arndt, S., Vanderborght, J.P., and Regnier, P.: Diatom growth response to physical forcing in a
1303 macrotidal estuary: Coupling hydrodynamics, sediment transport, and biogeochemistry.
1304 *Journal of Geophysical Research C: Oceans*, 112(5), 2007.
- 1305 Arndt, S. and Regnier, P.: A model for the benthic-pelagic coupling of silica in estuarine ecosystems:
1306 sensitivity analysis and system scale simulation, *Biogeosciences*, 4, 331–352, doi:10.5194/bg-
1307 4-331-2007, 2007.
- 1308 Arndt, S., Regnier, P., and Vanderborght, J.P.: Seasonally-resolved nutrient export fluxes and filtering
1309 capacities in a macrotidal estuary. *Journal of Marine Systems*, 78(1), 42-58, 2009.
- 1310 Arndt, S., Lacroix, G., Gypens, N., Regnier, P., and Lancelot, C.: Nutrient dynamics and phytoplankton
1311 development along an estuary-coastal zone continuum: A model study. *Journal of Marine*
1312 *Systems*, 84(3-4), 49-66, 2011.
- 1313 Atlas, R., Hoffman, R.N., Ardizzone, J., Leidner, S.M., Jusem, J.C., Smith, D.K. and Gombos, D.: A
1314 cross-calibrated, multiplatform ocean surface wind velocity product for meteorological and
1315 oceanographic applications. *Bulletin of the American Meteorological Society*, 92(2), 157-174,
1316 2011.
- 1317 Baklouti, M., Chevalier, C., Bouvy, M., Corbin, D., Pagano, M., Troussellier, M., and Arfi, R.: A study of
1318 plankton dynamics under osmotic stress in the Senegal River Estuary, West Africa, using a 3D
1319 mechanistic model, *Ecol. Model.*, 222, 2704–2721, 2011.
- 1320 Bauer, J.E., Cai, W.J., Raymond, P.A., Bianchi, T.S., Hopkinson, C.S., and Regnier, P.A.G.: The changing
1321 carbon cycle of the coastal ocean. *Nature*, 504(7478), 61-70, 2013.
- 1322 Beusen, A. H.W., Dekkers, A. L. M., Bouwman, A. F., Ludwig, W., and Harrison, J.: Estimation of global
1323 river transport of sediments and associated particulate C, N, and P, *Global Biogeochem. Cy.*,
1324 19, GB4S05, doi:10.1029/2005GB002453, 2005.
- 1325 Beusen, A.H.W., Bouwman, A.F., Dürr, H.H., Dekkers, A.L.M., and Hartmann, J.: Global patterns of
1326 dissolved silica export to the coastal zone: Results from a spatially explicit global model.
1327 *Global Biogeochemical Cycles*, 23, GB0A02, doi:10.1029/2008GB003281, 2009.
- 1328 | Borges, A.V., Delille, B., and Frankignoulle, M.: Budgeting sinks and sources of CO₂ in the coastal
1329 ocean: Diversity of ecosystems counts. *Geophys. Res. Lett.*, 32(14), L14601, 2005.
- 1330 Borges, A.V., and Abril, G.: Carbon Dioxide and Methane Dynamics in Estuaries. In: E. Wolanski and
1331 D.S. McLusky (Editors), *Treatise on Estuarine and Coastal Science*. Academic Press, Waltham,
1332 pp. 119–161, 2012.
- 1333 Bricker, S., Longstaff, B., Dennison, W., Jones, A., Boicourt, K., Wicks, C., and Woerner, J.: Effects of
1334 Nutrient Enrichment In the Nation's Estuaries: A Decade of Change, NOAA, MD, 2007.
- 1335 Brock, T.D.: Calculating solar radiation for ecological studies. *Ecological Modelling*, 14(1-2), 1-19,
1336 1981.
- 1337 Caffrey, J.: Factors controlling net ecosystem metabolism in U.S. estuaries. *Estuaries*, 27(1), 90-101,
1338 2004.
- 1339 Cai, W.J., and Wang, Y.: The chemistry, fluxes, and sources of carbon dioxide in the estuarine waters
1340 of the Satilla and Altamaha Rivers, Georgia. *Limnology and Oceanography*, 43(4), 657-668,
1341 1998.
- 1342 Cai, W.J., Wang, Y., and Hodson, R. E.: Acid-base properties of dissolved organic matter in the
1343 estuarine waters of Georgia, USA. *Geochimica et Cosmochimica Acta*, 62(3), 473-483, 1998.
- 1344 Cai, W.J., Pomeroy, L.R., Moran, M.A., and Wang, Y.: Oxygen and carbon dioxide mass balance for
1345 the estuarine-intertidal marsh complex of five rivers in the southeastern U.S. *Limnology and*
1346 *Oceanography*, 44, 639-649, 1999.

Deleted: Billen, G., Thieu, V., Garnier, J., and Silvestre, M.: Modelling the N cascade in regional waters: The case study of the Seine, Somme and Scheldt rivers, *Agr. Ecosyst. Environ.*, 133, 234–246, 2009.¶

1353 Cai, W.J.: Estuarine and coastal ocean carbon paradox: CO₂ sinks or sites of terrestrial carbon
1354 incineration? *Ann. Rev. Mar. Sci.*, 3, 123-145, 2011.

1355 Cerco, C., Kim, S.-C., and Noel, M.: The 2010 Chesapeake Bay eutrophication model. US
1356 Environmental Protection Agency Chesapeake Bay Program, Annapolis, MD, 2010.

1357 Chen, C.-T.A., Huang, T.-H., Fu, Y.-H., Bai, Y., and He, X.: Strong sources of CO₂ in upper estuaries
1358 become sinks of CO₂ in large river plumes. *Current Opinion in Environmental Sustainability*,
1359 4(2), 179-185, 2012.

1360 Chen, C.-T. A., Huang, T.-H., Chen, Y.-C., Bai, Y., He, X., and Kang, Y.: Air-sea exchanges of CO₂ in the
1361 world's coastal seas, *Biogeosciences*, 10, 6509–6544, doi:10.5194/bg-10-6509-2013, 2013.

1362 Dai, T., and Wiegert, R.G.: Estimation of the primary productivity of *Spartina alterniflora* using a
1363 canopy model. *Ecography*, 19(4), 410-423, 1996.

1364 Dür, H.H., Meybeck, M., and Dür, S.H.: Lithological composition of the Earth's continental surfaces
1365 derived from a new digital map emphasizing riverine material transfer. *Glob. Biogeochem.*
1366 *Cycles* 19 (4), GB4S10, 2005.

1367 Dür, H.H., Laruelle, G.G., van Kempen, C.M., Slomp, C.P., Meybeck, M., and Middelkoop, H.:
1368 Worldwide Typology of Nearshore Coastal Systems: Defining the Estuarine Filter of River
1369 Inputs to the Oceans. *Estuaries and Coasts*, 34(3), 441-458, 2011.

1370 EPA (2009). "1970 - 2008 Average annual emissions, all criteria pollutants in MS Excel." National
1371 Emissions Inventory (NEI) Air Pollutant Emissions Trends Data. Office of Air Quality Planning
1372 and Standards. Available online at <<http://www.epa.gov/ttn/chieftrends/index.html>>

1373 Fekete, B.M., Vörösmarty, C.J., and Grabs, W.: High-resolution fields of global runoff combining
1374 observed river discharge and simulated water balances. *Global Biogeochemical Cycles*, 16(3),
1375 15-1, 2002.

1376 Fischer, H. B.: Mixing and Dispersion in Estuaries, *Annu. Rev. Fluid Mech.*, 8, 107–133, 1976.

1377 Friedrichs, M.A.M., and Hofmann, E.E.: Physical control of biological processes in the central
1378 equatorial Pacific Ocean. *Deep-Sea Research Part I: Oceanographic Research Papers*, 48(4),
1379 1023-1069, 2001.

1380 Garcia, H.E., Locarnini, R.A., Boyer, E.W., Antonov, A., Baranova, O.K., Zweng, M.M., and Johnson,
1381 D.R.: *World Ocean Atlas 2009, Volume 3: Dissolved Oxygen, Apparent Oxygen Utilization,*
1382 *and Oxygen Saturation, 2010a.*

1383 Garcia, H.E., Locarnini, R.A., Boyer, E.W., Antonov, J.I., Baranova, O.K., Zweng, M.M., and Johnson,
1384 D.R.: *World Ocean Atlas 2009, Volume 4: Nutrients (phosphate, nitrate, silicate), 2010b.*

1385 Garnier, J., Servais, P., Billen, G., Akopian, M., and Brion, N.: Lower Seine River and Estuary (France)
1386 Carbon and Oxygen Budgets During Low Flow, *Estuaries*, 24, 964–976, 2001.

1387 [GRDC: Global Freshwater Fluxes into the World Oceans / Online provided by Global Runoff Data](#)
1388 [Centre. 2014 ed. Koblenz: Federal Institute of Hydrology \(BfG\), 2014.](#)

1389 Harrison, J.A., Caraco, N., and Seitzinger, S.P.: Global patterns and sources of dissolved organic
1390 matter export to the coastal zone: Results from a spatially explicit, global model. *Global*
1391 *Biogeochemical Cycles*, 19(4), GB4S03, doi:10.1029/2004GB002357, 2005.

1392 Hartmann, J., Jansen, N., Dür, H.H., Kempe, S., and Köhler, P.: Global CO₂ consumption by chemical
1393 weathering: What is the contribution of highly active weathering regions? *Global Planet.*
1394 *Change*, 69(4), 185-194, 2009.

1395 Hartmann, J., Dür, H.H., Moosdorf, N., Meybeck, M., and Kempe, S.: The geochemical composition
1396 of the terrestrial surface (without soils) and comparison with the upper continental crust.
1397 *Int. J. Earth Sci.* 101, 365-376, 2012.

1398 Herrmann, M., Najjar, R.G., Kemp, W.M., Alexander, R.B., Boyer, E.W., Cai, W.-J., Griffith, P.C.,
1399 Kroeger, K.D., McCallister, S.L., and Smith, R.A.: Net ecosystem production and organic
1400 carbon balance of U.S. East Coast estuaries: A synthesis approach, *Global Biogeochem.*
1401 *Cycles*, 29, doi:10.1002/2013GB004736, 2015.

1402 Hofmann, A.F., Soetaert, K., and Middelburg, J.J.: Present nitrogen and carbon dynamics in the
1403 Scheldt estuary using a novel 1-D model. *Biogeosciences*, 5(4), 981-1006, 2008.

Deleted: Dufore, C. M.: Spatial and Temporal Variations in the Air-Sea Carbon Dioxide Fluxes of Florida Bay, Graduate School Thesis, University of South Florida, 2012.¶

1409 Hofmann, E.E., Cahill, B., Fennel, K., Friedrichs, M.A.M., Hyde, K., Lee, C., Mannino, A., Najjar, R.G.,
1410 O'Reilly, J.E., Wilkin, J., and Xue, J.: Modeling the dynamics of continental shelf carbon. *Ann*
1411 *Rev Mar Sci.* 3, 93-122, 2011.

1412 Hunt, C. W., Salisbury, J. E., Vandemark, D., and McGillis, W.: Contrasting Carbon Dioxide Inputs and
1413 Exchange in Three Adjacent New England Estuaries. *Estuar. Coast.*, 34, 68–77,
1414 doi:10.1007/s12237-010-9299-9, 2010.

1415 Hunt, C.W., Salisbury, J.E., Vandemark, D., and McGillis, W.: Contrasting Carbon Dioxide Inputs and
1416 Exchange in Three Adjacent New England Estuaries. *Estuaries and Coasts*, 34(1), 68-77, 2011.

1417 Ippen, A.T., and Harleman, D.R.F.: One-dimensional Analysis of Salinity Intrusion in Estuaries,
1418 Technical Bulletin No. 5, Committee on Tidal Hydraulics, Corps of Engineers, US Army,
1419 Vicksburg, 1961.

1420 Jiang, L.Q., Cai, W.J., and Wang, Y.: A comparative study of carbon dioxide degassing in river- and
1421 marine-dominated estuaries. *Limnology and Oceanography*, 53(6), 2603-2615, 2008.

1422 Jiang, L.-Q., Cai, W.-J., Wang, Y., and Bauer, J. E.: Influence of terrestrial inputs on continental shelf
1423 carbon dioxide, *Biogeosciences*, 10, 839–849, doi:10.5194/bg-10-839-2013, 2013.

1424 Joesoef, A., Huang, W.-J., Gao, Y., and Cai, W.-J.: Air–water fluxes and sources of carbon dioxide in
1425 the Delaware Estuary: spatial and seasonal variability, *Biogeosciences*, 12, 6085-6101,
1426 doi:10.5194/bg-12-6085-2015, 2015.

1427 Kent, B.H.: Turbulent diffusion in a Sectionally Homogeneous Estuary, Technical Report 16,
1428 Chesapeake Bay Institute, John Hopkins, University, Baltimore, 1958.

1429 Key, R.M., Kozyr, A., Sabine, C.L., Lee, K., Wanninkhof, R., Bullister, J.L., Feely, R.A., Millero, F.J.,
1430 Mordy, C., and Peng, T.H.: A global ocean carbon climatology: Results from Global Data
1431 Analysis Project (GLODAP). *Global Biogeochemical Cycles*, 18(4), 1-23, 2004.

1432 Laruelle, G.G.: Quantifying nutrient cycling and retention in coastal waters at the global scale, Ph D
1433 dissertation, Utrecht University, 2009.

1434 Laruelle, G. G., Regnier, P., Ragueneau, O., Kempa, M., Moriceau, B., Ni Longphuir, S., Leynaert, A.,
1435 Thouzeau, G., and Chauvaud, L.: Benthic-pelagic coupling and the seasonal silica cycle in the
1436 Bay of Brest (France): new insights from a coupled physical-biological model, *Mar. Ecol.-*
1437 *Prog. Ser.*, 385, 15–32, 2009.

1438 Laruelle, G.G., Dürr, H.H., Slomp, C.P., and Borges, A.V.: Evaluation of sinks and sources of CO₂ in the
1439 global coastal ocean using a spatially-explicit typology of estuaries and continental shelves.
1440 *Geophys. Res. Lett.*, 37(15), L15607, doi:10.1029/2010GL043691, 2010.

1441 Laruelle, G.G., Dürr, H.H., Lauerwald, R., Hartmann, J., Slomp, C.P., Goossens, N., and Regnier, P.A.G.:
1442 Global multi-scale segmentation of continental and coastal waters from the watersheds to
1443 the continental margins. *Hydrol. Earth Syst. Sci.*, 17(5), 2029-2051, 2013.

1444 Laruelle, G.G., Lauerwald, R., Rotschi, J. Raymond, P.A., and Regnier, P.: Seasonal response of air-
1445 water CO₂ exchange along the land-ocean aquatic continuum of the northeast North
1446 American coast. *Biogeosci.* 12, 1447-1458, 2015.

1447 Lauerwald, R., Hartmann, J., Moosdorf, N., Kempe, S., and Raymond, P.A.: What controls the spatial
1448 patterns of the riverine carbonate system? — A case study for North America. *Chemical*
1449 *Geology*, 337–338, 114-127, 2013.

1450 Lauerwald, R., Laruelle, G. G., Hartmann, J., Ciais, P., and Regnier, P. A. G.: Spatial patterns in CO₂
1451 evasion from the global river network, *Global Biogeochem. Cy.*, 29, 534–554,
1452 doi:10.1002/2014GB004941, 2015.

1453 Leonard, B.: Third-Order Upwinding as a Rational Basis for Computational Fluid Dynamics, in:
1454 *Computational Techniques and Applications: CTAC-83*, edited by: Noye J. and Fletcher C. A.
1455 J., Elsevier, North-Holland, 1984.

1456 Le Quééré, C., Peters, G. P., Andres, R. J., Andrew, R. M., Boden, T. A., Ciais, P., Friedlingstein, P.,
1457 Houghton, R. A., Marland, G., Moriarty, R., Sitch, S., Tans, P., Arneeth, A., Arvanitis, A., Bakker,
1458 D. C. E., Bopp, L., Canadell, J. G., Chini, L. P., Doney, S. C., Harper, A., Harris, I., House, J. I.,
1459 Jain, A. K., Jones, S. D., Kato, E., Keeling, R. F., Klein Goldewijk, K., Körtzinger, A., Koven, C.,

1460 Lefèvre, N., Maignan, F., Omar, A., Ono, T., Park, G.-H., Pfeil, B., Poulter, B., Raupach, M. R.,
 1461 Regnier, P., Rödenbeck, C., Saito, S., Schwinger, J., Segschneider, J., Stocker, B. D., Takahashi,
 1462 T., Tilbrook, B., van Heuven, S., Viovy, N., Wanninkhof, R., Wiltshire, A., and Zaehle, S.:
 1463 Global carbon budget 2013, *Earth Syst. Sci. Data*, 6, 235-263, doi:10.5194/essd-6-235-2014,
 1464 2014.

1465 Le Quéré, C., Moriarty, R., Andrew, R. M., Canadell, J. G., Sitch, S., Korsbakken, J. I., Friedlingstein, P.,
 1466 Peters, G. P., Andres, R. J., Boden, T. A., Houghton, R. A., House, J. I., Keeling, R. F., Tans, P.,
 1467 Arneeth, A., Bakker, D. C. E., Barbero, L., Bopp, L., Chang, J., Chevallier, F., Chini, L. P., Ciais, P.,
 1468 Fader, M., Feely, R. A., Gkritzalis, T., Harris, I., Hauck, J., Ilyina, T., Jain, A. K., Kato, E., Kitidis,
 1469 V., Klein Goldewijk, K., Koven, C., Landschützer, P., Lauvset, S. K., Lefèvre, N., Lenton, A.,
 1470 Lima, I. D., Metzl, N., Millero, F., Munro, D. R., Murata, A., Nabel, J. E. M. S., Nakaoka, S.,
 1471 Nojiri, Y., O'Brien, K., Olsen, A., Ono, T., Pérez, F. F., Pfeil, B., Pierrot, D., Poulter, B., Rehder,
 1472 G., Rödenbeck, C., Saito, S., Schuster, U., Schwinger, J., Séférian, R., Steinhoff, T., Stocker, B.
 1473 D., Sutton, A. J., Takahashi, T., Tilbrook, B., van der Laan-Luijckx, I. T., van der Werf, G. R., van
 1474 Heuven, S., Vandemark, D., Viovy, N., Wiltshire, A., Zaehle, S., and Zeng, N.: Global Carbon
 1475 Budget 2015, *Earth Syst. Sci. Data*, 7, 349-396, doi:10.5194/essd-7-349-2015, 2015.

1476 Lin, J., Xie, L., Pietrafesa, L. J., Ramus, J. S., and Paerl, H.W.: Water Quality Gradients across
 1477 Albemarle-Pamlico Estuarine System: Seasonal Variations and Model Applications, *J. Coast.
 1478 Res.*, 23, 213–229, 2007.

1479 Locarnini, R.A., Mishonov, A.V., Antonov, J.I., Boyer, T.P., Garcia, H.E., Baranova, O.K., Zweng, M.M.,
 1480 and Johnson, D.R.: *World Ocean Atlas 2009, Volume 1: Temperature*, 2010.

1481 Ludwig, W., Probst, J. L., and Kempe, S.: predicting the oceanic input of organic carbon by
 1482 continental erosion, *Global Bio geochem. Cy.*, 10, 23–41, 1996.

1483 Maher, D.T., and Eyre, B.D.: Carbon budgets for three autotrophic Australian estuaries: Implications
 1484 for global estimates of the coastal air-water CO₂ flux. *Global Biogeochem. Cycles*, 26(1),
 1485 GB1032, 2012.

1486 Mateus, M., Vaz, N., and Neves, R.: A process-oriented model of pelagic biogeochemistry for marine
 1487 systems. Part II: Application to a mesotidal estuary, *J. Mar. Syst.*, 94, 90–101, 2012.

1488 Mayorga, E., Seitzinger, S.P., Harrison, J.A., Dumont, E., Beusen, A.H.W., Bouwman, A.F., Fekete,
 1489 B.M., Kroeze, C., and Van Drecht, G.: Global Nutrient Export from WaterSheds 2 (NEWS 2):
 1490 Model development and implementation. *Environmental Modelling and Software*, 25(7),
 1491 837-853, 2010.

1492 Meybeck, M.: Carbon, nitrogen, and phosphorus transport by world rivers. *Am. J. Sci.*, 282(4), 401-
 1493 450, 1982.

1494 Meybeck, M., Dürr, H. H., and Vörosmary, C. J.: Global coastal segmentation and its river catchment
 1495 contributors: A new look at land-ocean linkage, *Global Biogeochem. Cy.*, 20, GB1590,
 1496 doi:10.1029/2005GB002540, 2006.

1497 Middelburg, J.J., Klaver, G., Nieuwenhuize, J., Wielemaker, A., De Haas, W., Vlug, T., and Van Der
 1498 Nat, J.F.W.A.: Organic matter mineralization in intertidal sediments along an estuarine
 1499 gradient. *Marine Ecology Progress Series*, 132(1-3), 157-168, 1996.

1500 NASA/NGA: *SRTM Water Body Data Product Specific Guidance, Version 2.0*, 2003.

1501 Najjar, R.G., Friedrichs, M., and Cai, W.-J. (Editors): Report of The U.S. East Coast Carbon Cycle
 1502 Synthesis Workshop, January 19-20, 2012. Ocean Carbon and Biogeochemistry Program and
 1503 North American Carbon Program, 34 pp, 2012.

1504 Nihoul, J. C. J., and Roday, F.: Modèles d'estuaires partiellement stratifiés, *Projet Mer*, Vol. 10,
 1505 Service de la Programmation Scientifique, Bruxelles, Belgium, 71–98, 1976.

1506 Nixon, S.W., J.W. Ammerman, L.P. Atkinson, V.M. Berounsky, G. Billen, W.C. Boicourt, W.R. Boynton,
 1507 T.M. Church, D.M. Ditoro, R. Elmgren, J.H. Garber, A.E. Giblin, R.A. Jahnke, N.J. P. Owens,
 1508 M.E.Q. Pilson, and Seitzinger, S.P.: The fate of nitrogen and phosphorus at the land–sea
 1509 margin of the North Atlantic Ocean. *Biogeochemistry* 3, 141–180, 1996.

1510 NOAA: National Estuarine Inventory Data Atlas, Volume 1: Physical and Hydrologic Characteristics,
 1511 National Oceanic and Atmospheric Administration, MD, 1985.

1512 Odum, H.T.: Primary Production in Flowing Waters. *Limnol. Oceanogr.*, 1, 102-117, 1956.

1513 O’Kane, J. P.: Estuarine Water Quality Management. Pitman, London, U.K, 1980.

1514 Platt, T., Gallegos, C. L., and Harrison, W. G.: Photoinhibition of photosynthesis in natural
 1515 assemblages of marine phytoplankton. *J. Mar. Res.*, 38, 687-701, 1980.

1516 Preddy, W. S.: The mixing and movement of water in the estuary of the Thames, *J. Mar. biol. Ass. UK*,
 1517 33, 645–662, 1954.

1518 Press, W. H., Teukolosky, S. A., Vetterling, W. T., and Flannery, B.P.: Numerical Recipes in C: The Art
 1519 of Scientific Programming, 2nd Edn., Cambridge University Press, USA, 1992.

1520 Pritchard, D. W.: The Equations of Mass Continuity and Salt Continuity in Estuaries, *J. Marine Res.*,
 1521 15, 33–42, 1958.

1522 Raymond, P.A., Caraco, N.F., and Cole, J.J.: Carbon dioxide concentration and atmospheric flux in the
 1523 Hudson River. *Estuaries*, 20(2), 381-390, 1997.

1524 Raymond, P.A., Bauer, J.E., and Cole, J.J.: Atmospheric CO₂ evasion, dissolved inorganic carbon
 1525 production, and net heterotrophy in the York River estuary. *Limnology and Oceanography*,
 1526 45(8), 1707-1717, 2000.

1527 Raymond, P.A., and Hopkinson, C.S.: Ecosystem Modulation of Dissolved Carbon Age in a Temperate
 1528 Marsh-Dominated Estuary. *Ecosystems*, 6(7), 694-705, 2003.

1529 Raymond, P.A., Hartmann, J., Lauerwald, R., Sobek, S., McDonald, C., Hoover, M., Butman, D., Striegl,
 1530 R., Mayorga, E., Humborg, C., Kortelainen, P., Dürr, H., Meybeck, M., Ciais, P., and Guth, P.:
 1531 Global carbon dioxide emissions from inland waters. *Nature*, 503(7476), 355-359, 2013.

1532 Regnier, P., Wollast, R., and Steefel, C.I.: Long-term fluxes of reactive species in macrotidal estuaries:
 1533 Estimates from a fully transient, multicomponent reaction-transport model. *Marine*
 1534 *Chemistry*, 58(1-2), 127-145, 1997.

1535 Regnier, P., Mouchet, A., Wollast, R., and Ronday, F.: A discussion of methods for estimating residual
 1536 fluxes in strong tidal estuaries, *Cont. Shelf Res.*, 18, 1543–1571, 1998.

1537 Regnier, P., and Steefel, C.I.: A high resolution estimate of the inorganic nitrogen flux from the
 1538 Scheldt estuary to the coastal North Sea during a nitrogen-limited algal bloom, spring 1995.
 1539 *Geochimica et Cosmochimica Acta*, 63(9), 1359-1374, 1999.

1540 Regnier, P., Vanderborgh, J. P., Steefel, C. I., and O’Kane, J. P.: Modeling complex multi-component
 1541 reactive-transport systems: Towards a simulation environment based on the concept of a
 1542 Knowledge Base, *Appl. Math. Model.*, 26, 913–927, 2002.

1543 Regnier, P., Friedlingstein, P., Ciais, P., Mackenzie, F.T., Gruber, N., Janssens, I.A., Laruelle, G.G.,
 1544 Lauerwald, R., Luysaert, S., Andersson, A.J., Arndt, S., Arnosti, C., Borges, A.V., Dale, A.W.,
 1545 Gallego-Sala, A., Godderis, Y., Goossens, N., Hartmann, J., Heinze, C., Ilyina, T., Joos, F.,
 1546 LaRowe, D.E., Leifeld, J., Meysman, F.J.R., Munhoven, G., Raymond, P.A., Spahni, R.,
 1547 Suntharalingam, P., and Thullner, M.: Anthropogenic perturbation of the carbon fluxes from
 1548 land to ocean. *Nature Geosci*, 6(8), 597-607, 2013a.

1549 Regnier, P., Arndt, S., Goossens, N., Volta, C., Laruelle, G.G., Lauerwald, R., and Hartmann, J.:
 1550 Modelling Estuarine Biogeochemical Dynamics: From the Local to the Global Scale. *Aquatic*
 1551 *Geochemistry*, 19(5-6), 591-626, 2013b.

1552 Riemann, B., Simonsen, P., and Stensgaard, L.: The carbon and chlorophyll content of phytoplankton
 1553 from various nutrient regimes. *Journal of Plankton Research*, 11 (5), 1037-1045, 1989.

1554 Rossow, W.B., and Schiffer, R.A.: Advances in understanding clouds from ISCCP. *Bull. Amer.*
 1555 *Meteorol. Soc.*, 80, 2261-2288, doi:10.1175/1520-0477(1999)080<2261:AIUCFI>2.0.CO;2,
 1556 1999.

1557 Sarma, V.V.S.S., Viswanadham, R., Rao, G.D., Prasad, V.R., Kumar, B.S.K., Naidu, S.A., Kumar, N.A.,
 1558 Rao, D.B., Sridevi, T., Krishna, M.S., Reddy, N.P.C., Sadhuram, Y., and Murty, T.V.R.: Carbon
 1559 dioxide emissions from Indian monsoonal estuaries. *Geophysical Research Letters*, 39(3),
 1560 L03602, 2012.

Deleted: Paerl, H.W., Valdes, L.M., Peierls, B.L., Adolf, J.E., and Harding Jr, L.W.: Anthropogenic and climatic influences on the eutrophication of large estuarine ecosystems. *Limnology and Oceanography*, 51(1 II), 448-462, 2006.¶

1567 Savenije, H.H.G.: A one-dimensional model for salinity intrusion in alluvial estuaries. *Journal of*
1568 *Hydrology*, 85(1-2), 87-109, 1986.

1569 Savenije, H.H.G.: Lagrangian solution of St. Venant's equations for alluvial estuary. *Journal of*
1570 *Hydraulic Engineering*, 118(8), 1153-1163, 1992.

1571 Savenije, H. H. G. (Ed.): *Salinity and Tides in Alluvial Estuaries*, 1st Edn., Elsevier, Amsterdam, 2005.

1572 Savenije, H. H. G. (Ed.): *Salinity and Tides in Alluvial Estuaries*, 2nd Edn., available at:
1573 <http://salinityandtides.com> (last access: 8 March 2015), 2012.

1574 Seitzinger, S. P., Harrison, J. A., Dumont, E., Beusen, A. H. W., and Bouwman, A. F.: Sources and
1575 delivery of carbon, nitrogen, and phosphorus to the coastal zone: An overview of Global
1576 Nutrient Export from Watersheds (NEWS) models and their application, *Global Biogeochem.*
1577 *Cycles*, 19, GB4S01, doi:10.1029/2005GB002606, 2005.

1578 Schwarz, G.E., Hoos, A.B., Alexander, R.B., and Smith, R.A.: The SPARROW Surface Water-Quality
1579 Model: Theory, Application and User Documentation. U.S. Geological Survey, Techniques
1580 and Methods Report, Book 6, Chapter B3, Reston, Virginia, 2006

1581 Sharp, J. H., Yoshiyama, K., Parker, Schwartz, M. C., Curlless, S. E., Bearegard, A. Y., Ossolinski, J. E.,
1582 and Davis, A. R.: A Biogeochemical View of Estuarine Eutrophication: Seasonal and Spatial
1583 Trends and Correlations in the Delaware Estuary. *Estuaries and Coasts*, 32, 1023-1043,
1584 doi:10.1007/s12237-009-9210-8, 2009.

1585 Sharp, J. H.: Estuarine oxygen dynamics: What can we learn about hypoxia from long-time records in
1586 the Delaware Estuary? *Limnol. Oceanogr.*, 55(2), 2010, 535-548, 2010.

1587 Shih, J.-S., Alexander, R.B., Smith, R.A., Boyer, E.W., Schwarz, G.E., and Chung, S.: An initial SPARROW
1588 model of land use and in-stream controls on total organic carbon in streams of the
1589 conterminous United States, U. S. Geological Survey, Reston, Virginia, 2010.

1590 Signorini, S.R., Mannino, A., Najjar Jr, R.G., Friedrichs, M.A.M., Cai, W.J., Salisbury, J., Wang, Z.A.,
1591 Thomas, H., and Shadwick, E.: Surface ocean pCO₂ seasonality and sea-air CO₂ flux
1592 estimates for the North American east coast. *Journal of Geophysical Research C: Oceans*,
1593 118(10), 5439-5460, 2013.

1594 Simmons, H. B.: Some effects of inland discharge on estuarine hydraulics, *Proc. Am. Soc. Civ. Eng.-*
1595 *ASCE*, 81, 792, 1955.

1596 Soetaert, K., and Herman, P.M.J.: Nitrogen dynamics in the Westerschelde estuary (SW Netherlands)
1597 estimated by means of the ecosystem model MOSES. *Hydrobiologia*, 311(1-3), 225-246,
1598 1995.

1599 Stets, E.G., and Strieg, R.G.: Carbon export by rivers draining the conterminous united states. *Inland*
1600 *Waters*, 2(4), 177-184, 2012.

1601 Stigter, C., and Siemons, J.: Calculation of longitudinal salt distribution in estuaries as function of
1602 time, *Publication Delft Hydraulics Laboratory*, 52, The Netherlands, 1967.

1603 Tian, H., Chen, G., Liu, M., Zhang, C., Sun, G., Lu, C., Xu, X., Ren, W., Pan, S., and Chappelka, A.: Model
1604 estimates of net primary productivity, evapotranspiration, and water use efficiency in the
1605 terrestrial ecosystems of the southern United States during 1895-2007. *Forest Ecology and*
1606 *Management*, 259(7), 1311-1327, 2010.

1607 Tian, H., Chen, G., Zhang, C., Liu, M., Sun, G., Chappelka, A., Ren, W., Xu, X., Lu, C., Pan, S., Chen, H.,
1608 Hui, D., McNulty, S., Lockaby, G., and Vance, E.: Century-Scale Responses of Ecosystem
1609 Carbon Storage and Flux to Multiple Environmental Changes in the Southern United States.
1610 *Ecosystems*, 15(4), 674-694, 2012.

1611 U. S. Fish and Wildlife Service. 2014. National Wetlands Inventory website. U.S. Department of the
1612 Interior, Fish and Wildlife Service, Washington, D.C. <http://www.fws.gov/wetlands/>, last
1613 accessed: February 2015.

1614 Vanderborght, J.P., Wollast, R., Loijens, M., and Regnier, P.: Application of a transport-reaction
1615 model to the estimation of biogas fluxes in the Scheldt Estuary. *Biogeochemistry*, 59(1-2),
1616 207-237, 2002.

Deleted: Thieu, V., Mayorga, E., Billen, G., and Garnier, J.: Subregional and downscaled global scenarios of nutrient transfer in river basins: Seine-Somme-Scheldt case study. *Global Biogeochemical Cycles*, 24(2), 2010.¶

- 1623 Vanderborght, J.P., Folmer, I., Aguilera, D.R., Uhrenholdt, T., and Regnier, P.: Reactive-transport
1624 modelling of a river-estuarine-coastal zone system: application to the Scheldt estuary. *Mar.*
1625 *Chem.* 106, 92-110, 2007.
- 1626 Volta, C., Arndt, S., Savenije, H.H.G., Laruelle, G.G., and Regnier, P.: C-GEM (v 1.0): a new, cost-
1627 efficient biogeochemical model for estuaries and its application to a funnel-shaped system.
1628 *Geosci. Model Dev.*, 7, 1271-1295, doi:10.5194/gmd-7-1271-2014, 2014.
- 1629 Volta, C., Laruelle, G. G., and Regnier, P.: Regional carbon and CO₂ budgets of North Sea tidal
1630 estuaries, *Estuarine, Coastal and Shelf Science*, 176, 76-90, 2016a.
- 1631 Volta, C., Laruelle, G. G., Arndt, S., and Regnier, P.: Linking biogeochemistry to hydro-geometrical
1632 variability in tidal estuaries: a generic modeling approach, *Hydrol. Earth Syst. Sci.*, 20, 991-
1633 1030, doi:10.5194/hess-20-991-2016, 2016b.
- 1634 Vörösmarty, C.J., Fekete, B., and Tucker, B.A.: River Discharge Database, Version 1.0 (RivDIS v1.0),
1635 Volumes 0 through 6. A contribution to IHP-V Theme 1. Technical Documents in Hydrology
1636 Series. UNESCO, Paris, 1996.
- 1637 Wang, Z.A., and Cai, W.J.: Carbon dioxide degassing and inorganic carbon export from a marsh-
1638 dominated estuary (the Duplin River): A marsh CO₂ pump. *Limnology and Oceanography*,
1639 49(2), 341-354, 2004.
- 1640 [Zeebe, R. E. and Wolf-Gladrow, D. \(Eds.\): CO₂ in seawater: equilibrium, kinetics, isotopes, Elsevier,](#)
1641 [Amsterdam, 2001.](#)
- 1642

Deleted: Van der Burgh, P.:
Ontwikkeling van een methode voor het
voorspellen van zoutverdelingen in
estuaria, kanalen and zeeën,
Rijkswaterstaat Rapport, The
Netherlands, 1972.¶

Formatted: Space After: 0 pt

1649 **Table 1:** Estimates of total annual riverine input from watersheds to estuaries (Tg C yr⁻¹). The ranges
1650 are based on Stets and Striegl (2012), Global NEWS (Mayorga et al. 2010), Hartmann et al. (2009),
1651 SPARROW (Shih et al. 2010) and DLEM (Tian et al. 2010, 2012). Modified from Najjar et al. 2012.

	DIC	DOC	POC	TOTAL
NAR	0.2-0.8	0.3-2.1	0.1-0.2	0.6-3.1
MAR	1.4-1.8	0.5-2.3	0.1-0.3	2.0-4.4
SAR	0.4-1.4	0.9-1.6	0.1-0.2	1.4-3.2
TOTAL	2.0-4.0	1.7-6.0	0.3-0.7	4.0-10.7

1652

1653

1654

1655 **Table 2:** Published local annually averaged estimates of $\overline{FCO_2}$ in mol C m⁻² yr⁻¹ for estuaries along the
 1656 East coast of the US.”

Name	Lon	Lat	$\overline{FCO_2}$		Reference
			Observed.	Modeled	
Altamaha Sound	-81.3	31.3	32.4	72.7	Jiang et al. (2008)
Bellamy	-70.9	43.2	3.6	3.9	Hunt et al. (2010)
Cochecho	-70.9	43.2	3.1	3.9	Hunt et al. (2010)
Doboy Sound	-81.3	31.4	13.9	25.7	Jiang et al. (2008)
Great Bay	-70.9	43.1	3.6	3.9	Hunt et al. (2011)
Little Bay	-70.9	43.1	2.4	3.9	Hunt et al. (2011)
Oyster Bay	-70.9	43.1	4	3.9	Hunt et al. (2011)
Parker River estuary	-70.8	42.8	1.1	3.9	Raymond and Hopkinson (2003)
Sapelo Sound	-81.3	31.6	13.5	20.6	Jiang et al. (2008)
Satilla River	-81.5	31	42.5	25.7	Cai and Wang (1998)
York River	-76.4	37.2	6.2	8.1	Raymond et al. (2000)
Hudson River	-74	40.6	13.5	15.5	Raymond et al. (1997)

1657

1658

Formatted Table

Deleted: Florida Bay

1660 **Table 3:** State variables and processes explicitly implemented in CGEM.

State variables		
Name	Symbol	Unit
Suspended Particulate Mater	SPM	gL ⁻¹
Total Organic Carbon	TOC	μM C
Nitrate	NO ₃	μM N
Ammonium	NH ₄	μM N
Phosphate	DIP	μM P
Dissolved Oxygen	DO	μM O ₂
Phytoplankton	Phy	μM C
Dissolved Silica	dSi	μM Si
Dissolved Inorganic Carbon	DIC	μM C
Biogeochemical reactions		
Name	Symbol	Unit
Gross primary production	GPP	μM C s ⁻¹
Net primary production	NPP	μM C s ⁻¹
Phytoplankton mortality	M	μM C s ⁻¹
Aerobic degradation	R	μM C s ⁻¹
Denitrification	D	μM C s ⁻¹
Nitrification	N	μM N s ⁻¹
O ₂ exchange with the atmosphere	FO ₂	μM O ₂ s ⁻¹
CO ₂ exchange with the atmosphere	FCO ₂	μM C s ⁻¹
SPM erosion	E _{SPM}	gL ⁻¹ s ⁻¹
SPM deposition	D _{SPM}	gL ⁻¹ s ⁻¹

1661

1662

1663 **Table 4:** Yearly averaged surface area (*S*), fresh water discharge (*Q*), residence time (*Rt*), *FCO₂* and
 1664 *NEM* of all simulated estuaries.

long degrees	lat degrees	<i>S</i> km ²	<i>Q</i> m ³ s ⁻¹	<i>Rt</i> days	$\overline{FCO_2}$ mol C m ⁻² yr ⁻¹	\overline{NEM} mol C m ⁻² yr ⁻¹	<i>FCO₂</i> 10 ⁶ mol C yr ⁻¹	<i>NEM</i> 10 ⁶ mol C yr ⁻¹
NAR								
-67.25	44.75	7	38.5	15	3.7	-37.4	27	-270
-67.25	45.25	12	73.6	15	6.0	-56.7	71	-666
-67.25	45.25	12	73.6	15	13.8	-56.6	162	-666
-67.75	44.75	3	68.5	4	6.7	-63.5	23	-221
-68.25	44.75	14	69.5	19	4.1	-56.2	58	-791
-68.75	44.75	89	309.9	23	27.4	-58.2	2431	-5163
-69.75	44.25	50	626.6	5	32.3	-74.4	1607	-3703
-70.25	43.75	3	25.8	10	2.1	-21.0	7	-71
-70.75	41.75	288	103.6	958	5.0	-4.0	1428	-1146
-70.75	42.25	63	210.7	40	16.2	-32.9	1025	-2081
-70.75	42.75	17	105.8	3	56.3	-69.0	943	-1155
MAR								
-70.75	43.25	31	29.9	11	21.6	-37.4	662	-1146
-71.25	41.75	257	28.2	808	3.9	-2.5	997	-650
-71.75	41.25	21	112.4	4	35.2	-32.6	726	-672
-72.75	40.75	20	25.4	62	30.7	-21.1	623	-430
-72.75	41.25	10	142.5	2	150.8	-36.9	1578	-386
-72.75	41.75	55	476.6	3	55.9	-45.7	3088	-2523
-73.25	40.75	19	26.8	56	31.4	-28.4	608	-550
-74.25	40.75	1192	608.2	126	15.5	-11.8	18432	-14047
-75.25	38.25	399	80.5	172	13.9	-5.0	5558	-2016
-75.25	38.75	354	31.8	357	7.5	-3.0	2659	-1076
-75.25	39.75	1716	499.0	221	10.0	-7.8	17072	-13439
-75.75	39.25	224	18.3	434	7.5	-2.9	1685	-640
-76.25	39.25	3427	717.1	352	8.1	-5.1	27646	-17352
-76.75	37.25	586	272.3	74	15.0	-10.4	8810	-6084
-76.75	37.75	154	36.3	163	10.7	-6.6	1654	-1023
-76.75	39.25	59	71.2	29	48.6	-34.6	2862	-2038
-77.25	38.25	206	30.2	268	6.1	-3.3	1265	-676
-77.25	38.75	568	259.2	118	16.7	-10.8	9488	-6134
SAR								
-78.25	34.25	48	167.4	7	122.5	-62.4	5916	-3015
-79.25	33.25	47	56.3	42	43.4	-36.5	2056	-1728
-79.25	33.75	45	291.4	8	85.1	-78.7	3843	-3551
-79.75	33.25	25	33.8	15	37.9	-32.8	956	-828
-80.25	32.75	25	31.0	50	48.8	-42.5	1214	-1057
-80.25	33.25	92	75.5	61	62.7	-61.2	5769	-5625
-80.75	32.25	71	21.1	182	12.9	-7.0	918	-501
-80.75	32.75	164	63.1	95	20.6	-11.5	3372	-1879
-81.25	31.75	92	71.7	45	25.7	-20.9	2361	-1926
-81.25	32.25	130	379.8	11	51.7	-39.2	6732	-5097
-81.75	30.75	34	18.7	61	17.5	-14.7	602	-505
-81.75	31.25	130	17.7	294	5.5	-4.0	713	-523
-81.75	31.75	56	350.5	4	72.7	-67.4	4068	-3770

1665

1666 **Table 5:** Seasonal contribution to FCO_2 and NEM in each the sub-region. The seasons displaying the
 1667 highest percentages are indicated in bold. Winter is defined as January, February and March, Spring
 1668 as April, May and June and so on...

Region	S km^2	NEM $mol\ C\ y^{-1}$	winter %	spring %	summer %	fall %	FCO_2 $mol\ C\ y^{-1}$	winter %	spring %	summer %	fall %
NAR	<u>558</u>	$-16.3\ 10^9$	14.7	21.2	37.0	27.2	$7.2\ 10^9$	26.3	18.9	26.5	28.3
MAR	<u>9298</u>	$-72.2\ 10^9$	21.9	25.9	28.8	23.4	$108.3\ 10^9$	29.8	23.3	20.7	26.2
SAR	<u>959</u>	$-30.5\ 10^9$	24.6	20.9	30.3	24.2	$39.2\ 10^9$	26	23.4	27	23.6

Formatted Table

Formatted: Superscript

1669

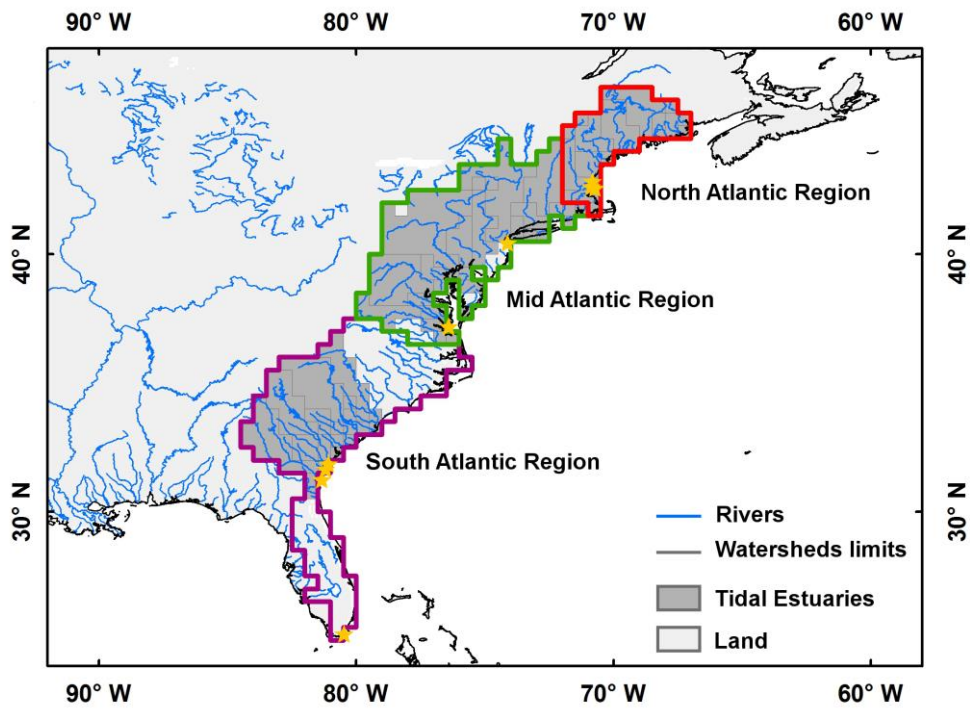
1670

1671 **Table 6:** Regressions and associated coefficient of determination between the depth normalized
 1672 residence time (S/Q) and $\overline{-NEM}/f(T)$, $\overline{FCO_2}/f(T)$ and $CFilt$.

Region	$\overline{-NEM}/f(T)$	$\overline{FCO_2}/f(T)$	$CFilt$
NAR	$y = 27.84 x^{-0.17}$ $r^2 = 0.11$	$y = 6.07 x^{0.00}$ $r^2 = 0.00$	$y = 15.08 \log_{10}(x) + 4.86$ $r^2 = 0.40$
MAR	$y = 26.03 x^{-0.63}$ $r^2 = 0.86$	$y = 34.36 x^{-0.58}$ $r^2 = 0.68$	$y = 40.46 \log_{10}(x) + 9.60$ $r^2 = 0.70$
SAR	$y = 28.36 x^{-0.71}$ $r^2 = 0.76$	$y = 32.82 x^{-0.66}$ $r^2 = 0.80$	$y = 23.19 \log_{10}(x) + 43.71$ $r^2 = 0.46$
MAR + SAR	$y = 25.85 x^{-0.64}$ $r^2 = 0.82$	$y = 31.64 x^{-0.58}$ $r^2 = 0.70$	$y = 33.30 \log_{10}(x) + 24.88$ $r^2 = 0.57$
NAR + MAR + SAR	$y = 28.98 x^{-0.66}$ $r^2 = 0.82$	$y = 12.98 x^{-0.33}$ $r^2 = 0.30$	$y = 40.64 \log_{10}(x) + 11.84$ $r^2 = 0.70$

1673

1674



1675

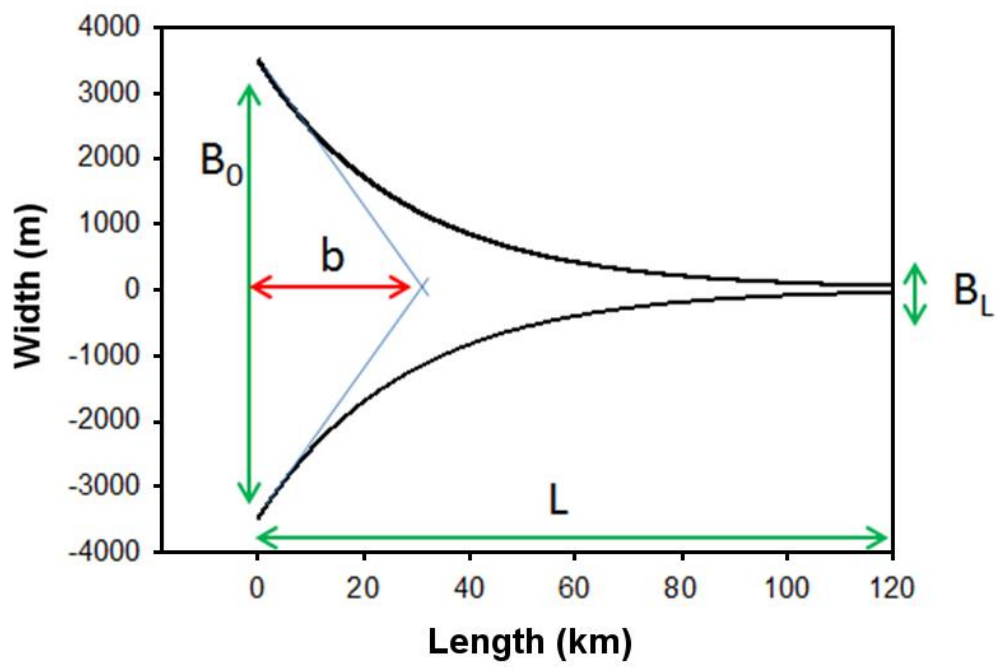
1676

1677

1678

1679

Figure 1: Limits of the 0.5 degrees resolution watersheds corresponding to tidal estuaries of the East coast of the US. 3 sub-regions are delimited with colors and orange stars represent the location of previous studies.

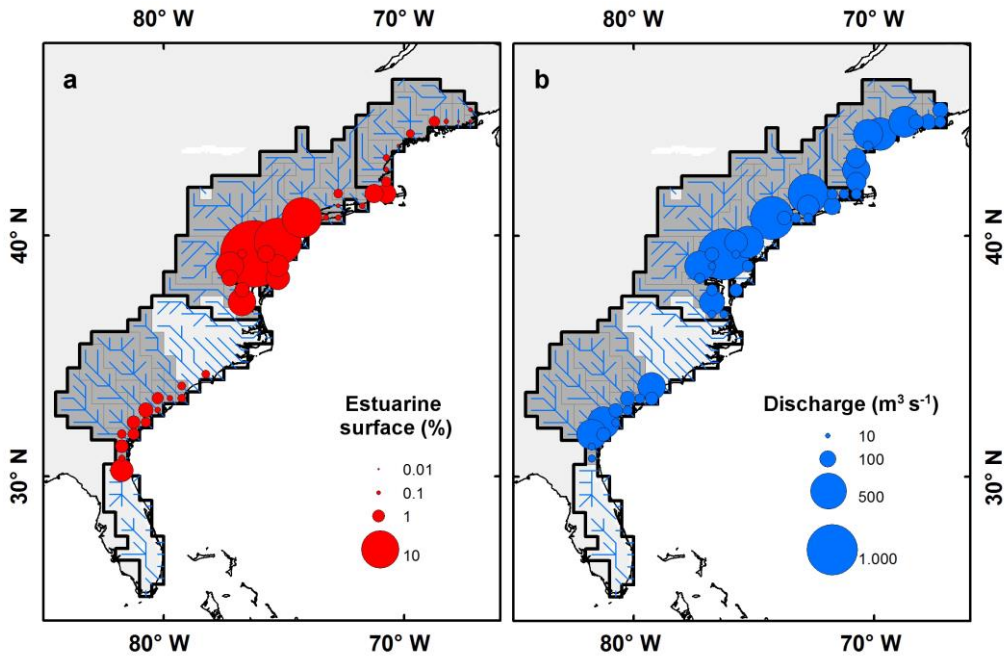


1680

1681 **Figure 2:** Idealized estuarine geometry and main parameters. Parameters indicated by green arrows
 1682 are measured, b is calculated. See section 2.3.1 for further details.

1683

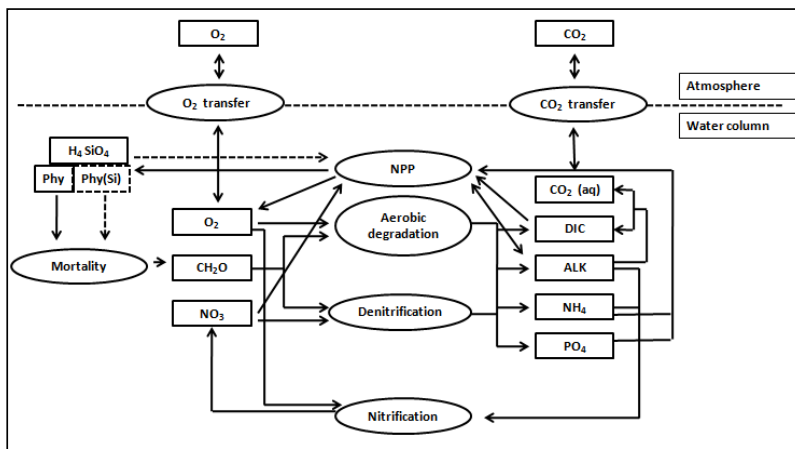
1684



1685

1686 **Figure 3:** Estuarine surface area (a) and mean annual freshwater discharge (b) for each tidal estuary
1687 of the East coast of the US. Estuarine surface area are expressed as percentage of the entire surface
1688 area of the region (19830 km²)

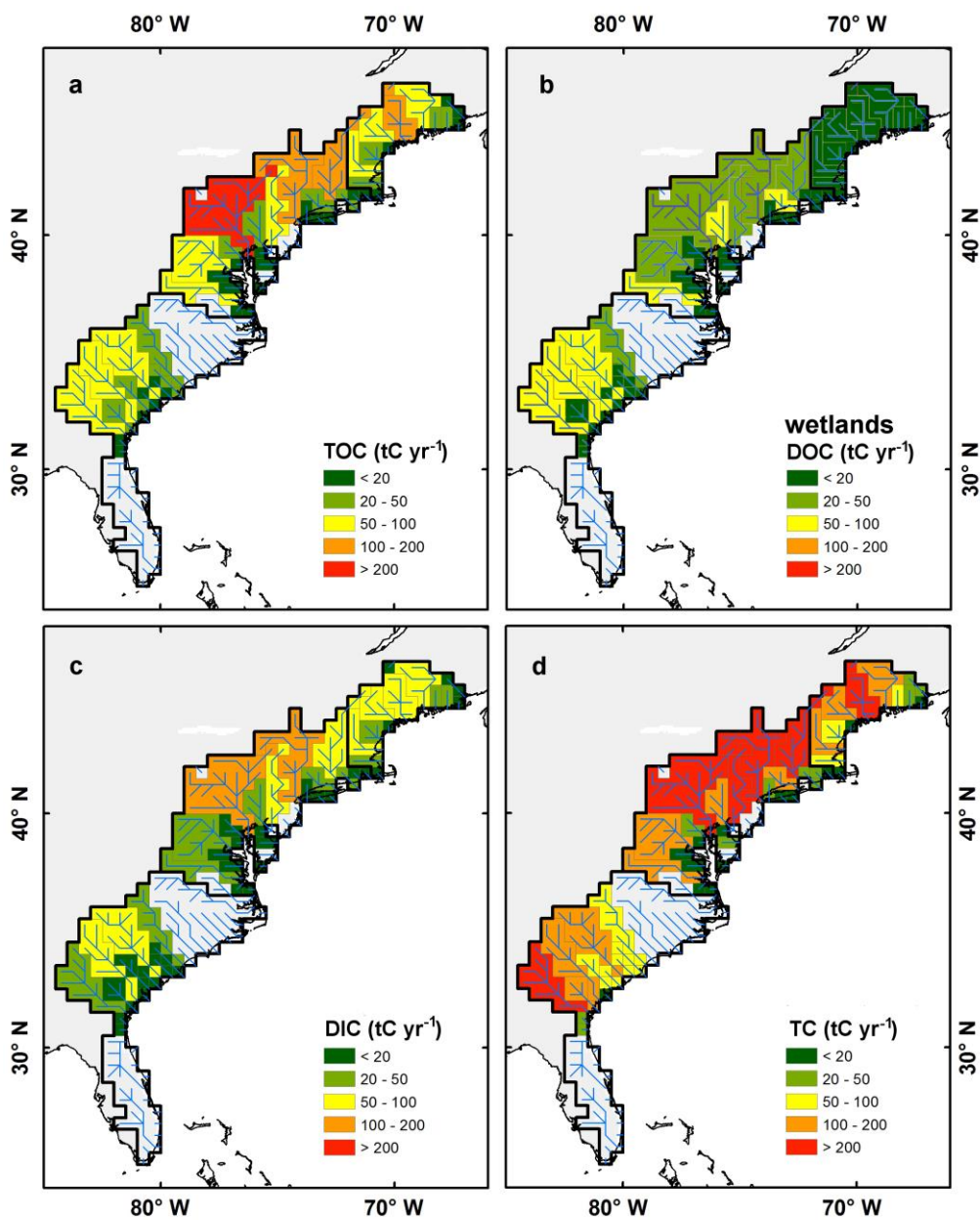
1689



1690

1691 **Figure 4:** Conceptual scheme of the biogeochemical module of C-GEM used in this study. State-
 1692 variables and processes are represented by boxes and oval shapes, respectively. Modified from Volta
 1693 et al., 2014.

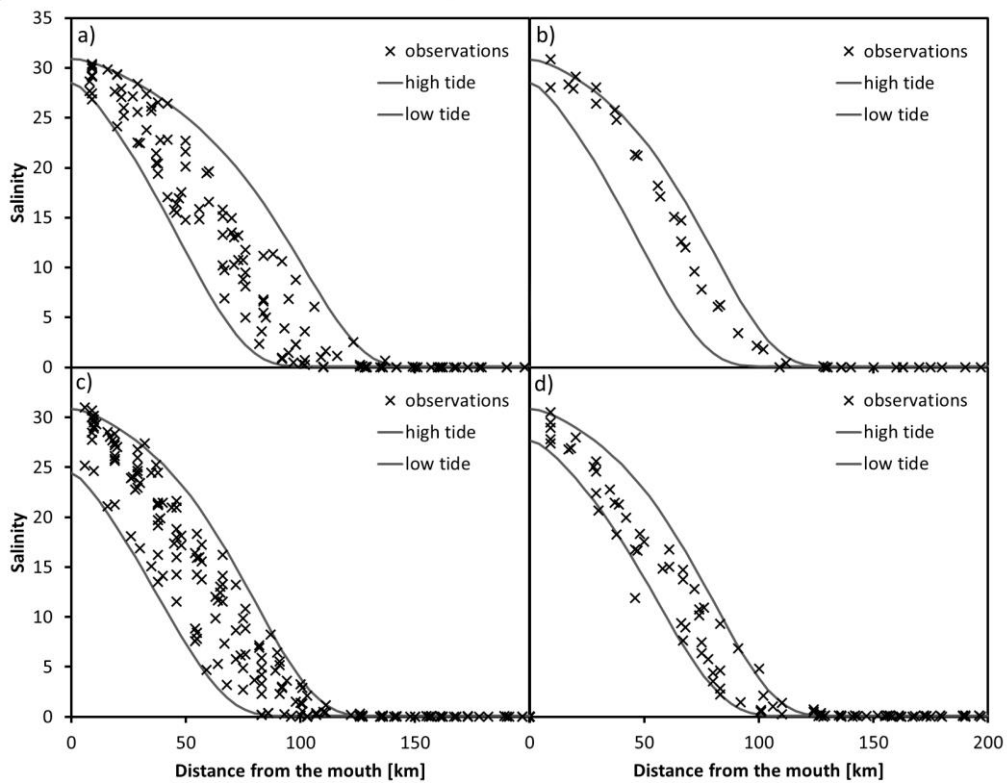
1694



1695

1696 **Figure 5:** Annual river carbon loads of TOC (a), annual DOC fluxes from wetlands (b), annual river
 1697 carbon loads of DIC (c) and annual TC fluxes (d). All fluxes are indicated per watershed.

1698



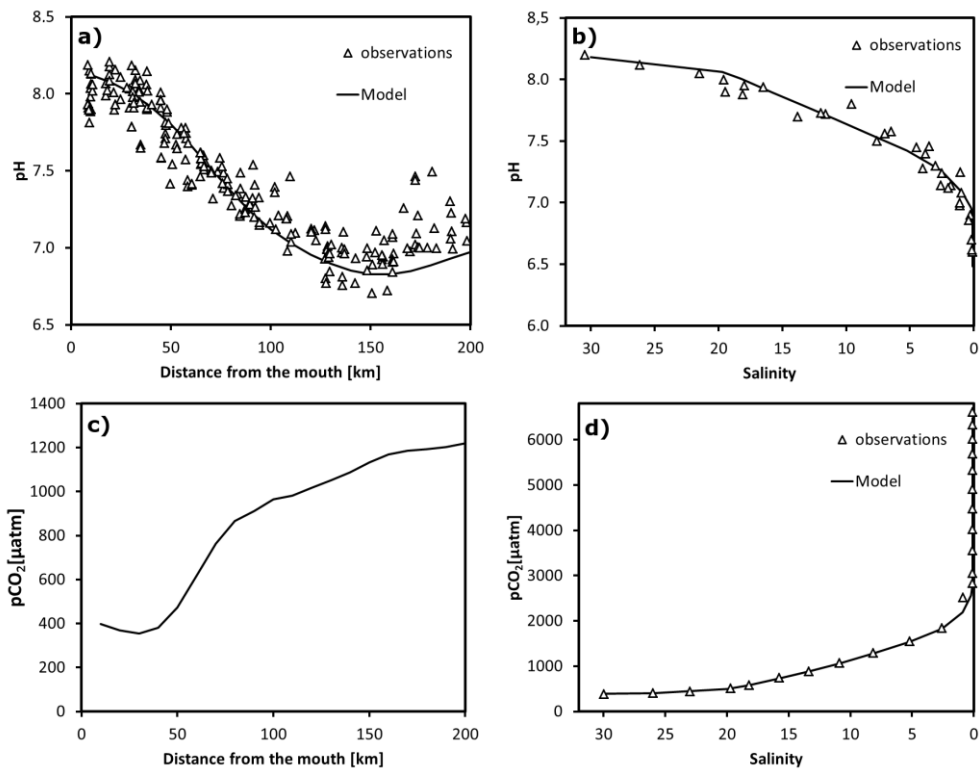
1699

1700 **Figure 6.** Modeled (lines) and measured (crosses) salinities in the Delaware Bay estuary for January

Formatted: No underline

1701 (a), February (b), May (c), June (d). The two lines correspond to high and low tides.

1702

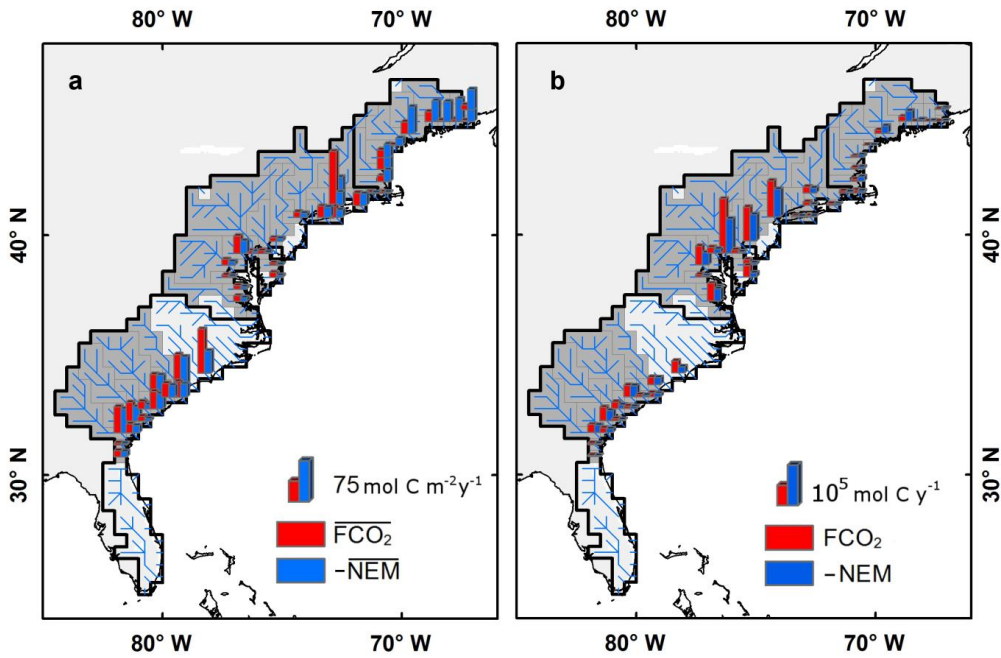


1703

1704 **Figure 7.** Longitudinal profiles of pH (top) and pCO₂ (bottom) for the Delaware Bay (left) and
 1705 Altamaha river estuary (right).

1706

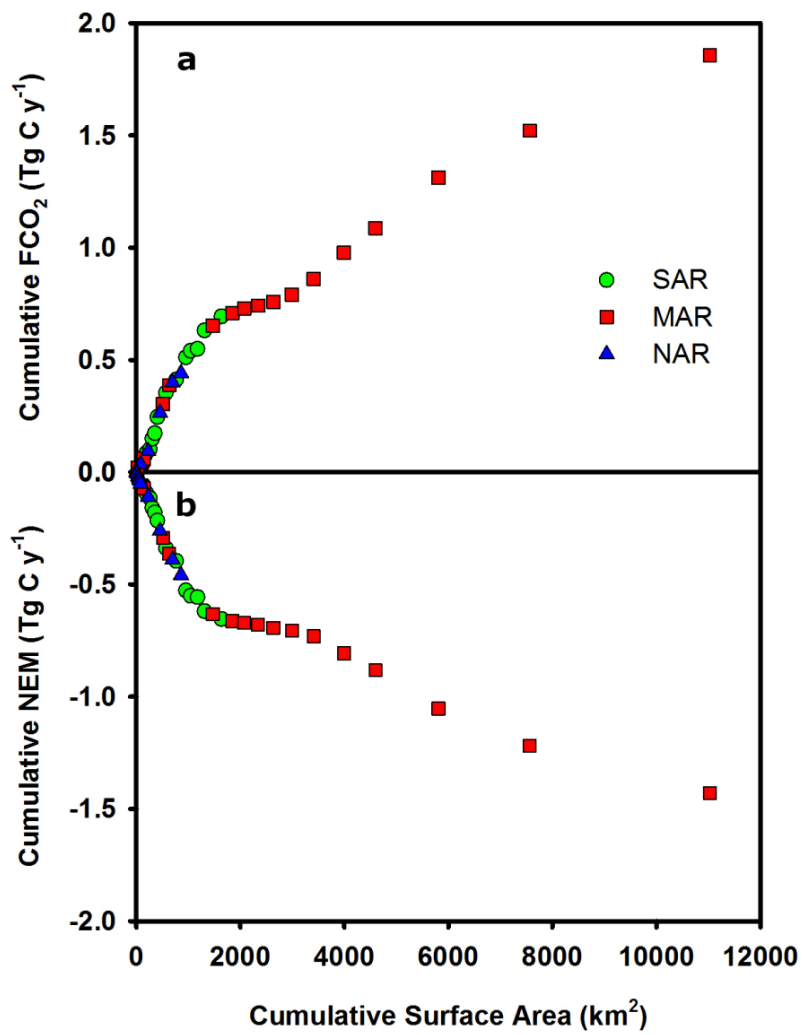
1707



1708

1709 **Figure 8:** Spatial distribution of spatially averaged value (a) and integrated value (b) of mean annual
1710 $\overline{FCO_2}$ (red) and $-\overline{NEM}$ (blue) along the East coast of the US. On panel a, the notation with overbars
1711 ($\overline{FCO_2}$ and $-\overline{NEM}$) represents rates per unit surface. For the sake of the comparison with $\overline{FCO_2}$, Fig.
1712 8 displays $-\overline{NEM}$ because the model predicts that all estuaries in this region are net heterotrophic.

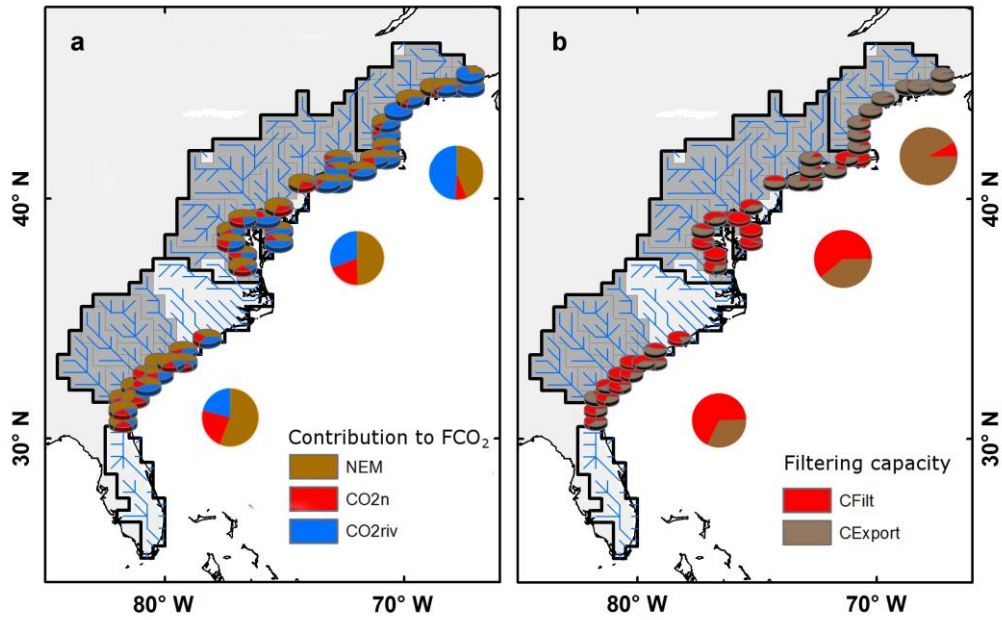
1713



1714

1715 **Figure 9:** The Cumulative FCO_2 (a) and NEM (b) as functions of the cumulative estuarine surface area.
 1716 Systems are sorted by increasing surface area.

1717

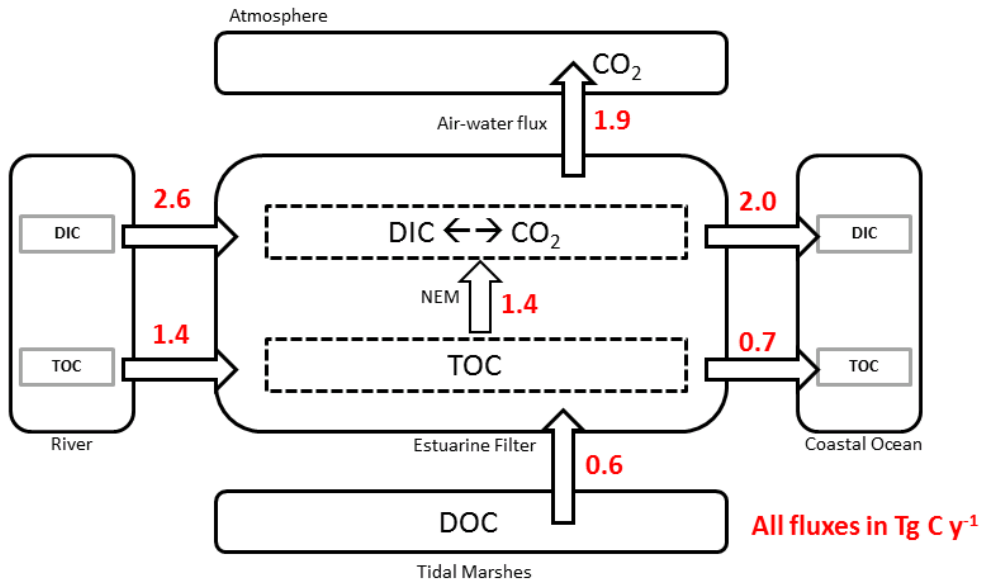


1718

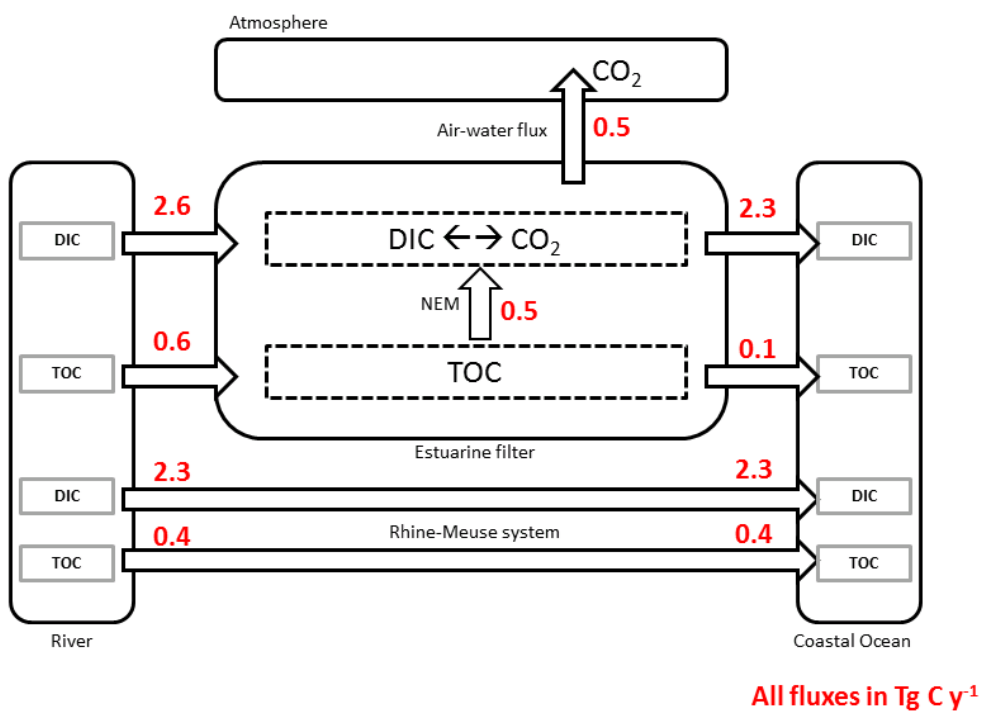
1719 **Figure 10:** Contribution of *NEM*, nitrification and riverine waters super-saturated waters to the mean
 1720 annual FCO_2 (a). Spatial distribution of mean annual carbon filtration capacities (*CFilt*) and export
 1721 (*CExport*) along the East coast of the US (b).

1722

a) Eastern US coast

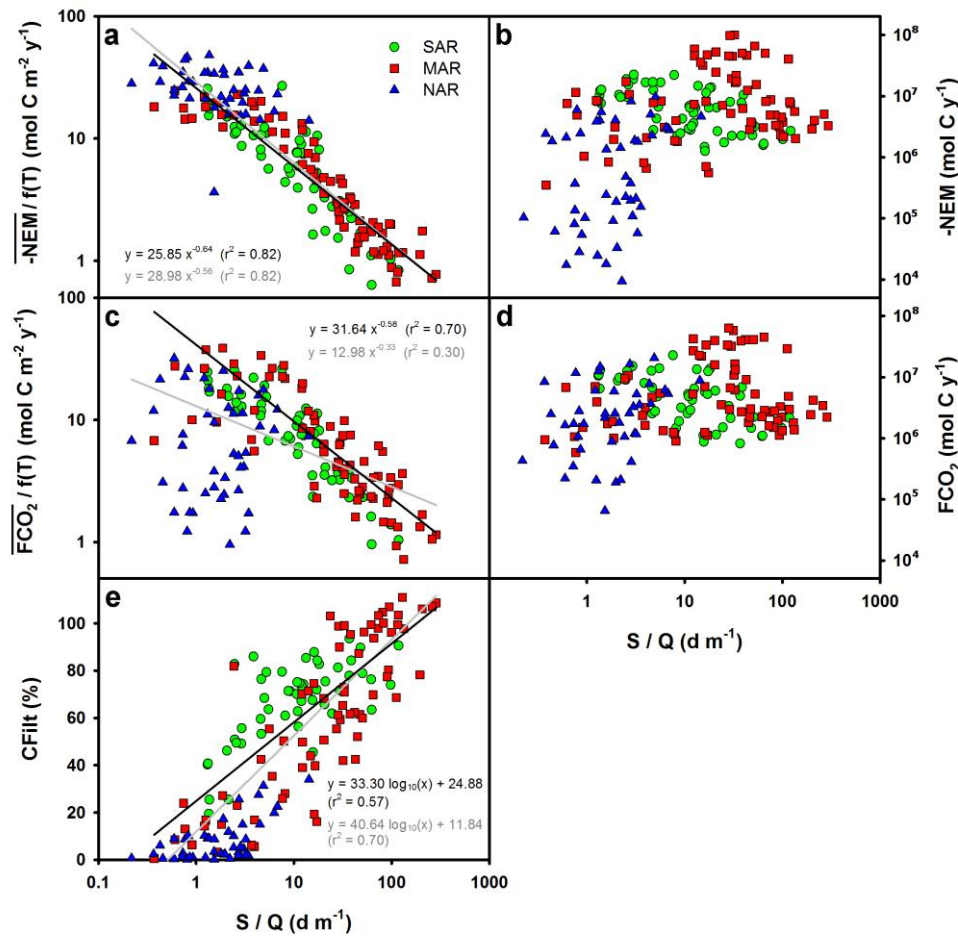


b) North Sea coast



1723

1724 **Figure 11:** Annual carbon budget of the estuaries of the East coast of the US (a) and of the coast of
 1725 the North Sea (b, modified from Volta et al., 2016a).



1726

1727 **Figure 12:** System scale integrated biogeochemical indicators expressed as functions of the depth
 1728 normalized residence time expressed as the ratio of the estuarine surface S and the river discharge Q
 1729 for all seasons. Panels b, d and e represent $\overline{-NEM}$, $\overline{FCO_2}$ and CFilt, respectively. Panels a and c
 1730 represent $\overline{-NEM}$, $\overline{FCO_2}$ normalized by a temperature Q_{10} function. Black lines are the best fitted linear
 1731 regressions obtained using all the point. Grey lines are best fit using only the estuaries from the MAR
 1732 and SAR regions.

1733

Deleted: -

Deleted: -

Deleted: -